Exp Fluids (2017) 58:108
DOI 10.1007/s00348-017-2386-y

REVIEW ARTICLE

A review of solid–fluid selection options for optical-based measurements in single-phase liquid, two-phase liquid–liquid and multiphase solid–liquid flows

Stuart F. Wright[1] · Ivan Zadrazil[1] · Christos N. Markides[1]

Received: 1 November 2016 / Revised: 16 March 2017 / Accepted: 5 June 2017 / Published online: 2 August 2017

Abstract Experimental techniques based on optical measurement principles have experienced significant growth in recent decades. They are able to provide detailed information with high-spatiotemporal resolution on important scalar (e.g., temperature, concentration, and phase) and vector (e.g., velocity) fields in single-phase or multiphase flows, as well as interfacial characteristics in the latter, which has been instrumental to step-changes in our fundamental understanding of these flows, and the development and validation of advanced models with ever-improving predictive accuracy and reliability. Relevant techniques rely upon well-established optical methods such as direct photography, laser-induced fluorescence, laser Doppler velocimetry/phase Doppler anemometry, particle image/tracking velocimetry, and variants thereof. The accuracy of the resulting data depends on numerous factors including, importantly, the refractive indices of the solids and liquids used. The best results are obtained when the observational materials have closely matched refractive indices, including test-section walls, liquid phases, and any suspended particles. This paper reviews solid–liquid and solid–liquid–liquid refractive-index-matched systems employed in different fields, e.g., multiphase flows, turbomachinery, bio-fluid flows, with an emphasis on liquid–liquid systems. The refractive indices of various aqueous and organic phases found in the literature span the range 1.330–1.620 and 1.251–1.637, respectively, allowing the identification of appropriate combinations to match selected transparent or translucent plastics/polymers, glasses, or custom materials in single-phase liquid or multiphase liquid–liquid flow systems. In addition, the refractive indices of fluids can be further tuned with the use of additives, which also allows for the matching of important flow similarity parameters such as density and viscosity.

✉ Christos N. Markides
c.markides@imperial.ac.uk

[1] Department of Chemical Engineering, Imperial College London, South Kensington Campus, London SW7 2AZ, UK

1 Introduction

This paper reviews the practice of refractive-index matching (RIM) in experimental work concerned with at least one liquid as the base fluid and excluding systems with a gaseous phase, thus focusing on solid–liquid and liquid–liquid combinations for use in two-phase liquid–liquid and multiphase solid–liquid flows, while retaining applicability to single-phase liquid flow systems. The main aim of this paper, given the significant recent developments in experimental techniques and the availability of solid materials and fluid substances, is to act as an updated, comprehensive resource that consolidates important optical data along with other relevant information on a large number of suitable solid and fluid options currently available for selection, and to provide broader guidance to experimentalists performing detailed, high-fidelity, accurate RIM optical-based measurements in the aforementioned fluid-flow systems. Information is included on aspects such as safety, toxicity, material compatibility, the role of temperature, solubility/miscibility, and more, as well as the use of liquid mixtures and additives (e.g., salts) for the tuning of properties such as density, viscosity, and surface/interfacial tension.

Multiphase interfacial flows consist of two or more immiscible phases, wherein a phase can be either a gas, liquid, or solid. Multiphase flows are of crucial importance in many diverse settings and applications across a wide range of scales including, but not limited to, flows in biological

and biomedical systems, atmospheric and marine environments, geological processes such as volcanic flows and landslides, planetary atmospherics, as well as processes in the oil and gas, petrochemical, energy, nuclear, transport, automotive, manufacturing, and food production industries. In particular, multiphase flows are encountered in important processes such as evaporation, condensation, boiling, mixing, reaction, cavitation, erosion, sedimentation, and extraction. Liquid–liquid flows are multiphase flows that consist of only two immiscible liquid, e.g., aqueous and organic, phases. The liquid phases can be present in these flows in a number of different so-called regimes, e.g., (i) stratified or stratified-wavy flows possibly with droplets of either or both phases at or near the interface, which are often encountered in oil and gas transportation lines; (ii) dispersed emulsions, which are common in dairy and chocolate processing, and power generation engines and plants; and (iii) combined emulsions and suspensions, e.g., in paint production. Despite their ubiquitous and important practical relevance, these flows are inherently complex, nonlinear, and multiscale in nature and remain poorly understood.

Optical diagnostic techniques are some of the most established flow-measurement methods. The collection of reliable quantitative data, however, has been dependent on the development of systems necessary for the rapid illumination and associated detection or imaging of interrogated flow regions, including lasers, cameras, photodetectors, etc., as well as the processing capabilities to perform semi-automatic processing of the resulting data. These capabilities only started to become available in the 1970s, which has led to a rapid increase in the evolution and use of these techniques. In particular, state-of-the-art experimental studies of multiphase flows can be performed using advanced non-intrusive, spatiotemporally resolved optical techniques, such as:

(i) Laser-induced fluorescence (LIF), as described by Kinsey (1977), Liu et al. (1977), Walker (1987) and Crimaldi (2008), has been used to provide phenomenological insight as well as quantitative information on the distribution and other key characteristics of the fluid phases, including phase fraction, wave amplitude and frequency, bubble size distribution and frequency, etc. LIF has been utilized in RIM systems by Diez et al. (2005), Ovdat and Berkowitz (2006), Liu et al. (2006a, b), Ravelet et al. (2007), Wu et al. (2011), Zadrazil et al. (2014), Zadrazil and Markides (2014), amongst others.

(ii) Laser Doppler velocimetry (LDV), laser/phase Doppler anemometry (LDA/PDA), and similar approaches have been detailed by Durst et al. (1976, 1997), Buchhave et al. (1979), Tropea (1995), Albrecht et al. (2003) and Czarske (2006). These methods allow the measurement of local velocity and/or droplet size within an interrogated volume and have been used in RIM systems by Varty (1984), Yarlagadda and Yoganathan (1989), Walker et al. (1989), Liu et al. (1989), Duncan et al. (1990), Chen and Kadambi (1990), Wildman et al. (1992), Koh et al. (1994), Jana (1995), Perktold et al. (1997), Dietze et al. (2009), and others.

(iii) Particle image/tracking velocimetry (PIV/PTV) and variants thereof have been covered in detail by Adrian (1986, 1991), Arroyo and Greated (1991), Maas et al. (1993), Grant (1997) and Fu et al. (2015), among others. These techniques can provide velocity information in two or three dimensions (2-D/3-D) and have been used in many RIM systems, e.g., by Northrup et al. (1991), Peurrung et al. (1995), Zachos et al. (1996), Hopkins et al. (2000), Longmire et al. (2001), Bale-Glickman et al. (2003), Ninomiya and Yasuda (2006), Burgmann et al. (2009), Dietze et al. (2009) Buchmann et al. (2010), Berard et al. (2013), Im et al. (2013), Yagi et al. (2013), Morgan et al. (2013), Zadrazil and Markides (2014), Krug et al. (2014).

In addition, less involved but equally important in providing (semi-)qualitative insight into the flows of interest is direct (high-speed) imaging, based on which a wealth of phenomenological information has been generated allowing significant advancements in relevant fields. All the aforementioned techniques have been presented here in the context of multiphase flow measurements; nevertheless, similar issues apply to internal single-phase (liquid) flows, both internal and external when walls are present, since optical distortions can occur at the solid–liquid interfaces (walls), limiting access to near-wall regions.

These optical methods have gained popularity, thanks to several advantages that they offer compared to more classical techniques for multiphase flow measurement and characterization, such as hot-wire/hot-film anemometry (Ueda and Tanaka 1975; Majithia et al. 2008), parallel/twin-wire, or conductivity probes (Han et al. 2006; Zhao et al. 2013). In particular, optical techniques: (i) can provide both qualitative and detailed high-resolution quantitative information on important flow phenomena and quantities; and (ii) are non-intrusive, so that these flow characteristics can be measured without introducing external disturbances to the flow. The main challenge when implementing for these techniques, however, is the requirement for optically undisturbed or fully known optical paths throughout the interrogated region, covering all fluid phases and any suspensions that may be of interest, including of the illumination and/or the observation or detection (e.g., reflected, scattered, and fluorescent) light. Specifically, optical distortions and intensity variations in the fluid domains under observation can arise due to the refraction and/or reflection of light when this

passes through materials with differing refractive indices (RIs), i.e., solid–gas, liquid–gas, solid–liquid, and liquid–liquid, depending on the fluids/flows of interest. These distortions lead to unwanted optical warping, displacement, and rotation of the measuring plane or volume, giving rise to increased errors in the measurement of interfacial topologies, velocities, or other scalars. This is typically addressed in the experimental design stage by the minimization of curved, angled, and uneven surfaces with the use of correction boxes similar to that shown in Fig. 1. Further improvements can be achieved by placing and then imaging pre-defined graticule targets in the measurement region like that shown in Fig. 2. The resulting images of these targets can then be used for spatial corrections during post-processing. Examples of the graticule correction method can be found in Zadrazil et al. (2012) in single-phase (liquid) circular pipe flows, and Morgan et al. (2013, 2016) in two-phase (liquid–liquid) pipe flows. Nevertheless, these corrections and, therefore, the associated errors can be minimized by selecting solid materials and liquid substances that have closely matching RIs, a practice which is known as refractive-index matching (RIM). The technique of refractive-index matching limits the physical process that causes refraction as well as reflection between differing materials.

The refraction of light at an interface is caused by a variation in the optical speed in the two adjacent transmission media, which creates a directional change in the propagation light path. The degree of change of the light path direction depends on the angle of incidence and the relative difference in the optical speeds in the two transmission media. The speed of light in a transmission medium v can be stated relative to the speed of light in a vacuum c, through the refractive index (RI), as defined by the following equation:

$$n = \frac{c}{v}, \tag{1}$$

based on which, Snell's law, also known as is the law of refraction and given in Eq. 2, relates a light ray's angle of incidence to its angle of refraction at the interface between two transmission media of differing RIs (here, n_1 and n_2; see also Fig. 3):

$$\frac{\sin(\theta_1)}{\sin(\theta_2)} = \frac{n_2}{n_1}. \tag{2}$$

It emerges from Snell's law that larger directional changes (distortions) occur at an interface when: (i) there are greater relative RI mismatches between the two transmission media; and (ii) the incident angle (relative to the interface normal direction) is large, as illustrated in Fig. 3a–c. Importantly, this also means that a higher RI mismatch or incident angle can lead to greater measurement errors if not fully corrected. Furthermore, if light travels from a material of higher RI (n_1) to one of lower RI (n_2), then a critical angle θ_c exists at which light travels along the interface (Fig. 3d), and beyond which the light is fully reflected (Fig. 3e) creating areas that are optically inaccessible. Snell's law can be used to determine this critical angle θ_c, as given by the following equation:

$$\theta_c = \arcsin\left(\frac{n_2}{n_1}\right). \tag{3}$$

In summary, the optical illumination of a targeted region of interest or its observation through interfaces (liquid–liquid or solid–liquid) associated with mismatched RIs can introduce positional or intensity uncertainty, and even lead

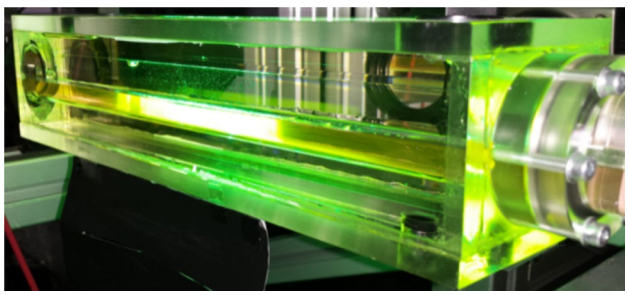

Fig. 1 Optical correction box illuminated by a laser sheet and containing a test pipe which is both filled and surrounded by an RI-matched (RI = 1.459) fluid. In this case, the pipe material is fused quartz and the oil Exxsol D140

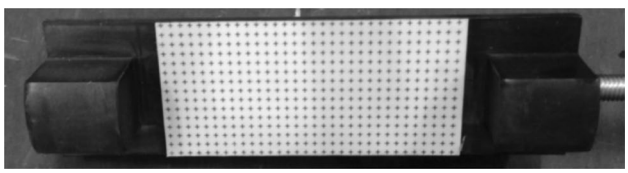

Fig. 2 Graticule (printed target) for the spatial calibration of images, e.g., within circular pipes

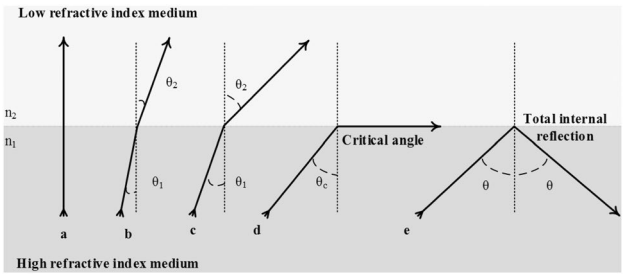

Fig. 3 Refraction of light at an interface as it passes from a high to a low RI medium: *a* no refraction/reflection occurs when the light direction is perpendicular to the interface; *b* slight refraction at low angles; *c* increasing refraction at higher angles; *d* critical angle between refraction and reflection; and *e* total internal reflection

to the observation of multiple images or optically inaccessible regions, especially if the interfaces are moving or curved. Such problems were reported, e.g., by Lowe and Kutt (1992), who were motivated to develop a spatial correction method using images from two cameras and ray tracing equations.

It should be noted that the RI and thus the angle of refraction are wavelength dependent, and this can lead to varying degrees of optical distortion depending on the wavelength if monochromatic light is used, or dispersion if mixed wavelength light is used; in fact, this forms the basis of some measurement methods. For example, in the case of the most common liquid, pure water, the RI shows rational function dependency on the wavelength in the visible part of the electromagnetic spectrum, with values in the range 1.330–1.343 for wavelengths 405–707 nm at 20 °C/1 bar(a) (Thormahlen et al. 1985). By convention, reported RIs are often measured using the sodium D-line at 598 nm; however, common lasers employed in optical-based measurements emit at different wavelengths (e.g., $\lambda_{Nd:YAG} = 266$, 532, 1064 nm; $\lambda_{Nd:YLF} = 527$ nm). This can induce errors in RI matching, since the RI of a solid phase or a liquid phase generally decreases with increasing wavelength (Forziati 1950), even in RIM systems that have been matched at their literature-reported values. Patil and Liburdy (2012) found that the use of fluorescent-dye doped seeding-particles introduced a further source of error, because the emitted fluorescent-light wavelengths differed to that of the laser source, and for which the system was optimized.

Beyond the illumination and/or observation wavelengths, a number of experimental parameters can lead to changes in the RIs of individual materials/substances in optical fluid-flow measurements, thus increasing errors even for initially matched systems in quiescent and laboratory-controlled environments, in particular, variations in temperature or pressure. Mondy et al. (1986) reported that the temperature had to be kept within ±1 °C to observe through 0.15 m of a 30% concentrated solid suspension, due to the temperature dependence of the RI of the fluid. This is an important consideration given that, unless controlled, the temperature can easily vary during experiments due to changes to the ambient conditions or the presence of heat sources or sinks in the flow loop (e.g., pumps or uninsulated walls). Significant temperature gradients leading to RI variations that introduce measurement errors were mentioned by Schmidt et al. (1984) who needed to create a laser-path correction curve to reduce positional errors in their LDA measurements in a fluid with a large temperature gradient. RI deviations can also occur through processes such as hygro-scopicity or evaporation causing relative changes to the components within fluid mixtures. In one example, Miller et al. (2006) found that the RI of their DEP and ethanol mixture changed over time due to the differential evaporation of the ethanol, highlighting the need for closed systems and fluid loops especially when dealing with volatile fluids. Similarly, changes can occur when the solid materials can absorb the liquid phase(s), leading to RI changes over time (Dijksman et al. 2012), or due to the chemical instability or reactivity of the materials employed, again, unless these are controlled by the experimental design and procedure. For instance, Averbakh et al. (1997) and Shauly et al. (1997) utilized a mixture of 14.1 wt% 1,1,2,2-tetrabromoethane, 35.7 wt% polyalkylene glycol oil, 50.3 wt% Triton X100, and 0.1 wt% Tinuvin 328 to match the RI of PMMA. In this example, the Tinuvin 328 was specifically added to the mixture to reduce the rate of UV breakdown of tetrabromoethane. Finally, the RIs of solid components can also vary due to non-uniformities introduced during their manufacture, such as material impurities, inclusions, etc.

Over and above the issues above relating directly to the differences in the RIs, the size of the measurement errors due to RI mismatches depends on many factors including the number of interfaces to the point of measurement and whether these are moving, the quantities being measured, the selected technique, the characteristics of the optical configuration and of the equipment used, and the experimental procedure and post-processing methods. The measurement error for a given fluid RI mismatch can, therefore, only be determined once all these factors have been taken into consideration. Consider, for example, two different types of flow of interest with identical optical setups and methods; in stratified liquid–liquid flows with a single, continuous, and stable interface, large RI differences can be tolerated for high-accuracy measurements, whereas in a finely dispersed liquid–liquid flow or a concentrated solid–liquid suspension, much closer RI matching would be required to achieve similar accuracies for the same measured quantities.

Nevertheless, particle position and consequent PIV measurement errors caused by mismatched RIs were considered by Patil and Liburdy (2010, 2012), who measured optical distortions in flows through packed beds and through porous media with RI differences as low as 0.0005. Two main types of distortion were identified in the former: (i) image centroid distortion due to refraction; and (ii) image intensity distortion, while in porous media, RI mismatching was found to give rise to the formation of multiple particle images, and relative PIV errors amounting to 2 and 4% for absolute RI differences of 0.0016 and 0.0036, respectively. Dijksman et al. (2012) found, experimentally, that imaging through 15 layers of 3-mm glass spheres was limited to a maximum RI mismatch of about 0.003 due to light scatter, and performed a numerical ray tracing exercise to quantify the effect of RI mismatching between the liquid and solid particles, finding that a standard deviation of 0.001 in the

spread of the particle RI created the same level of image blur as a RI mismatch of 0.002. Ray tracing also showed that considerable blurring was present through 25 layers when the RI was mismatched by 0.002. The same authors also noted that the RIs of particles are not normally given to the 0.2% accuracy required for RIM, and, therefore, that in situ RI matching was needed in their case. Furthermore, according to Hannoun (1985), RI differences as small as 0.0001 can affect LDV measurements through 30 cm of RI fluctuations, while Daviero et al. (2001) calculated that differences as low as 0.00005 may be needed for 40 cm of RI fluctuations. Hirsch et al. (2015) found that surface roughness, scratches, inclusions, fractures, inhomogeneity, and other manufacturing effects in plastics and glasses can all lead to measurement errors even for apparent perpendicular surfaces; some of these effects were directional causing the magnitude of the error to be depending on the surface axis.

Important parameters beyond optical clarity and accuracy also need to be considered when selecting liquids and solids for a given experiment, including densities and viscosities, non-Newtonian rheological behaviour where applicable, interfacial tension, and surface wettability, which is dependent on the surface energy balance between all fluid and solid phases, and quantified by the contact angle. Figure 4 demonstrates the definition of the contact angle for two fluid droplets on a solid surface in an immersion fluid. The fluid of droplet (a) on the left is more phobic of the surface than the immersion fluid and, therefore, has a larger contact angle, while the fluid of droplet (b) on the right has a greater affinity for the surface than the immersion fluid and so has a smaller contact angle. In particular, surface and interfacial tension should be taken into account when selecting fluids for liquid–liquid flow studies to match the experimental conditions in a given application (e.g., flow of water and oil through crude-oil transport pipelines).

Moreover, low reactivity and mutual solubility are desired, the latter being important in preventing the liquid–liquid interface becoming indeterminate. Similarly, the presence of surfactants in either fluid phase, whether

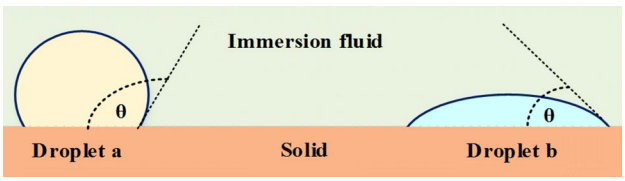

Fig. 4 Two droplets on a solid surface in a lighter emersion fluid (*gas* or *liquid*) making contact angles θ with a solid. The *liquid* of droplet (**a**) has a lower affinity for the surface than the immersion fluid and, therefore, has a large contact angle, while the *liquid* of droplet (**b**) has a greater affinity for the solid than the immersion fluid and so has a smaller contact angle

intentionally or not, can lead to the formation of emulsions and cause surface effects such as varying surface and interfacial tension across position and time. Finally, stability, toxicity, flammability, compatibility, and laser power tolerance should all be considered and carefully controlled. The design guidelines for liquid–liquid flow systems of Smedley and Coles (1990) are particularly useful here. Generalizing these guidelines, it is suggested: (i) not to use any system components, liquids or solids, that are unstable, reactive either between themselves or with the environment (air, flow loop components, etc.); (ii) not to use liquids that either damage, absorb, or dissolve any experimental solids or components of solids like plasticizers; (iii) not to use chemicals or optical components that undergo photodissociation or damage especially at wavelengths and powers used in light sources/lasers; (iv) to use safe, low-toxicity, and low-flammability chemicals whenever practicably possible; (v) to use materials that are optically transparent at all experimental wavelengths; (vi) to avoid liquids with high vapour-pressures or that are hydroscopic, thus reducing RI changes due to evaporation or absorption; (vii) to select low-cost fluid options; (viii) to select liquids that match the RI of the observations solids (walls, particles); and (ix) to select solids and liquids that give any desired contact angles. In the case of liquid–liquid systems, specifically, select the components for each phase to: (i) have low interphase solubility; (ii) allow matching over the required range of viscosities and densities; (iii) allow matching over a wide range of RIs to extend the options for the observational solid; and (iv) provide the desired interfacial tension between the liquids.

Four comprehensive papers have been published on RIM systems (Smedley and Coles 1990; Budwig 1994; Wiederseiner et al. 2011; Dijksman et al. 2012). Smedley and Coles (1990) created 121 single-component (pure) immiscible liquid–liquid pairs, some of which had closely matched RIs; however, none of these RIM pairs were based on the common fluids of water, glycerol, or silicone oil, and were not RI tuned as both liquids were single-component. Budwig (1994) detailed the principles of RIM liquid flows covering both single-phase liquid and two-phase liquid–liquid flows. Wiederseiner et al. (2011) reviewed the RIM literature for flows containing concentrated particle suspensions and covered solid–liquid systems in great detail, including techniques for matching the RI of solid particles and liquids. Dijksman et al. (2012) reviewed dense granular RIM systems for use with 3-D tomographic techniques whilst detailing the optical effect of RI mismatches in such systems. The tomographic method relied on laser scanning to build 3-D data of the granular material through the RIM system. Importantly, to the best of our knowledge, no publication to date has focused specifically on and documented earlier liquid–liquid and multiphase solid–liquid flow systems.

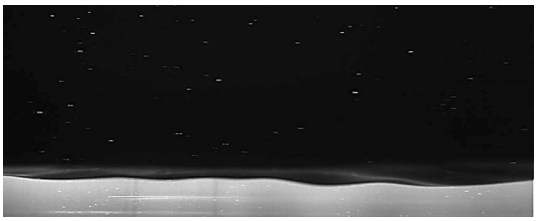

Fig. 5 Raw image from laser illumination in a stratified-wavy Exxsol D140 oil and water flow, showing planar LIF (PLIF) from the added dye in the water phase at the *bottom* of the pipe and particles for PIV/PTV in both *liquid* phases

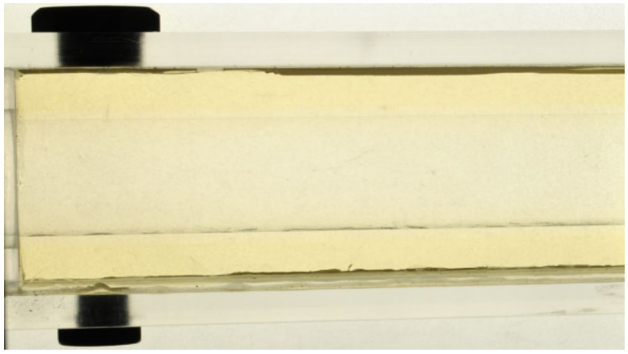

Fig. 6 Fused quartz pipe located inside a correction box with RIM liquid Exxsol D140 (RI = 1.459) both surrounding the *box* and within the pipe

By means of clarification, in some liquid–liquid RIM systems, only one of the liquids is matched to the solid, while the other is unmatched (e.g., due to other experiment design restrictions). Figure 5 shows such a system with Exxsol D140 oil and water. The oil is matched to the quartz pipe section at a RI of 1.459, whilst the water is unmatched with a RI of 1.333, resulting in distortions at the interface and in the water layer when viewing the flow from the bottom of the pipe; see the ghost-like reflections that are present around the liquid–liquid interface in the figure. For the purposes of this review, this type of liquid–liquid system is treated as if it is a solid–liquid RIM system (Sect. 2), and only systems where both liquids are matched are treated as liquid–liquid RIM systems (Sect. 3). These liquid–liquids RIM systems are then optionally matched to a solid material (Sect. 3.2).

The paper is organized as follows: Sect. 2 reviews solid–liquid RIM systems; Sect. 3 reviews liquid–liquid and solid–liquid–liquid RIM systems; Sect. 4 discusses liquid options and further RI tuning. Finally, conclusions are drawn in Sect. 5.

2 Solid–liquid systems

This section reviews solid–liquid flow systems that have previously been utilized in RIM experiments, i.e., matching the RI of a particular solid with either a pure liquid, a mixture of liquids, or additive solutions. Solid–liquid systems can be understood here as a suspension of particles in a liquid continuum (e.g., flow of a sand slurry) or a single-phase flow (e.g., external flow over a solid obstacle or internal flow within a pipe or conduit). An example of a solid–liquid system is given in Fig. 6, and consists of a 32-mm fused quartz pipe inside a correction box, where the box and pipe are both filled by a RIM Exxsol D140 oil (RI = 1.459).

A large number of solid–liquid RIM systems have been previously employed and so for clarity, these are separated into the following four sub-sections: Sect. 2.1 deals with common plastics; Sect. 2.2 considers silicone and urethane rubbers; Sect. 2.3 reports on custom polymers, resins, and hydrogels; and finally, Sect. 2.4 focuses on glasses.

2.1 Common plastics

Plastics are a common material for conducting RIM experiments. Many plastics are transparent or translucent when in the amorphous state, while the transparency of plastics in the crystalline state can sometimes be improved through transitioning to a more transparent amorphous state through heating above the melting temperature and quenching (Wiederseiner et al. 2011). Plastics are also readily available, affordable and can be easily manufactured in many different shapes and sizes. Consequently, they are preferentially chosen for the study of flows in complex geometries, e.g., biological systems, moving machinery, etc. (Soranna et al. 2008; Bale-Glickman et al. 2003). Two manufacturing processes are commonly used for the production of plastic components (e.g., test sections) that are commonly employed in scientific studies, namely extrusion and casting; more recently, rapid prototyping and 3-D printing processes have allowed an even greater range of components to be made from suitable plastics. Depending on the process, plastic components often bear different physical properties, despite their chemical composition being the same. Plastic pipes are frequently produced via extrusion processes, which can result in a ribbed effect on the pipe walls and a variability (and asymmetry) in the pipe diameter. Nevertheless, plastic pipes typically have a roughness of ~1 μm, which is much smoother than steel pipes frequently installed in industrial (e.g., the oil-and-gas) systems that have a roughness of 10s of μm (Hydraulic-Institute 1979).

Plastics vary widely in chemical composition and, as a result, important properties like air–water–solid contact angles θ (see Fig. 4) can span a wide range of values. For example, Nylon 6 has $\theta = 70°$ (Fort 1964), while the highly hydrophobic fluorocarbon polytetrafluoroethylene (PTFE)

has $\theta = 118°$ (Zhang et al. 2004). Plastics also vary in chemical resistance, so compatibility with contacting fluids should be checked carefully, since any incompatibility can lead to damage to the test section or other components in the flow loop. Dijksman et al. (2012) found that poly(methyl methacrylate) (PMMA) can develop microcracks when washed and dried after being in contact with Triton X100. Nevertheless, the chemical resistance of plastics can, in some cases, be improved. In the case of microcracks in PMMA, this can be done by reducing internal stresses through annealing after cutting (Hendriks and Aviram 1982). Further chemical compatibility issues encountered in the literature are discussed in the corresponding material section. Apart from chemical damage, physical damage can also occur from lasers, and this can occur at relatively low laser powers in some plastics, such as polycarbonate and PMMA [e.g., compared to glass, Hirsch et al. (2015)]. While this is mainly a consideration when using high-powered lasers, it should still be reviewed for a given experiment, especially if high luminosities are required.

This section focuses on solid–liquid matched RI systems, where the solid phase consists of a plastic material. The following plastics are considered, in order of increasing RI: fluorinated ethylene propylene (FEP), poly(vinyl acetate) (PVA), PMMA, nylon, and polystyrene (PS). In addition, previously unused, but common, plastics that could be utilized in future RIM experiments are included, namely: tetrafluoroethylene–hexafluoropropylene–vinylidene fluoride (THV), ethylene–tetrafluoroethylene (ETFE) and polyvinylidene difluoride (PVDF). Collated data of a number of possible solid–liquid RIM combinations, together with the known density and viscosity values of pure or fluid mixtures, can be found in Table 1.

Referring to Table 1, we proceed here to provide details relating to the various solid plastic materials, along with dedicated examples of their use in RIM systems. FEP is a hydrophobic fluorpolymer with a RI of 1.338, a density of 2150 kg/m^3, an air–water contact angle of $\theta = 102.1°$ (Akinci and Cobanoglu 2009), and has good chemical resistance. At optical wavelengths, FEP is translucent rather than clear, yet despite this, good images can still be taken through FEP walls a few mm thick. Importantly, the RI of FEP is close to that of water (1.333), and as a result, FEP has been implemented extensively as a RIM solid with water. For example, Satake et al. (2015) performed holographic PTV measurements in a sphere-packed pipe using a RIM system with water as the test fluid, an FEP pipe (RI = 1.338), and spheres were made from MEXFLON resin (RI = 1.330). The pipe was located in a square observation section filled with water (correction box) to reduce distortions from the outside pipe wall.

PVA is a rubbery polymer with a RI of about 1.470, a density of 1190 kg/m^3, and an air–water contact angle of $\theta = 60.6°$ (McCafferty and Wightman 1999). A fluid mixture of Pale 4 oil (oxidized castor oil) and tetrabromoethane was created by Karnis et al. (1966) to match the RI of PVA discs with RI = 1.467. This RIM system was used for the optical study of dilute, disc-shaped particle suspensions in Couette and Poiseuille flows. The authors reported satisfactory results with PVA in their application.

PMMA, which is also known by the trade names Perspex, Plexiglas, or acrylic glass, is the most commonly employed solid in RIM experiments with a RI of ≈ 1.490, a density of 1180 kg/m^3, and an air–water contact angle of $\theta = 59.3°$ (Stöhr et al. 2003). It is optically clear and is easily machined, although it is also brittle and prone to cracking. It has been used for optical measurements in RIM systems with complex geometries, e.g.: a model of abdominal aortic aneurysms (Budwig et al. 1993; Egelhoff et al. 1999); a column containing dispersed beads (Haam and Brodkey 2000; Haam et al. 2000); an axial turbo-pump (Uzol et al. 2002, 2007); or highly concentrated (50%) spherical suspensions (Breedveld et al. 1998, 2001, 2002; Breedveld 2000). PMMA can, however, be attacked by a number of chemicals, and hence, liquid compatibility must be carefully considered. Chemicals including ethanol (and other alcohols), dimethylsulfoxide (DMSO), and Triton X100 can all cause PMMA to form microcracks (Dijksman et al. 2012). In a related study, Liu et al. (1990) found that stress cracks and crazing created in PMMA by a mixture of 68.2 vol% turpentine oil and 31.8 vol% Tetralin (RI = 1.489) could be removed by a careful casting, machining and subsequent annealing treatment. Similarly, Jana (1995) treated PMMA with a silicon-based hard coating to increase its chemical resistance to Triton X100, which despite causing crazing is a close RI match to PMMA. Figure 7b shows a rod of PMMA immersed in Triton X100 with an RI of 1.489, and for contrast, Fig. 7a shows the same PMMA rod in air. Terpineol also attacks PMMA over long time scales, as observed Mondy et al. (1986) who matched PMMA to a mixture of 33.7 wt% polyalkylene glycol oil, 41.8 wt% terpineol, 24.4 wt% 1,1,2,2-tetrabromoethane, and 0.1 wt% Tinuvin. Furthermore, Dijksman et al. (2012) noted that PMMA is known to absorb water and found that it will also absorb Triton X100 as well as dimethylsulfoxide, and that this absorption leads to changes in the RI of PMMA, while Lyon and Leal (1998a) found that the RI of their quaternary liquid mixture was affected due to the differential absorption of the 1,6-dibromohexane mixture component into PMMA particles. Numerous liquids have been utilized for the matching of PMMA's RI, including aqueous salt solutions, and binary and ternary mixtures. A list of PMMA RIM systems along with density and viscosity information can be found in Table 1.

Nylon is translucent plastic, like FEP, with an RI of about 1.510, a density of about 1150 kg/m^3 and has an

Table 1 List of plastics and polymer-based RIM systems including: FEP, THV, ETFE, PVDF, PVA, PMMA, nylon, and PS

Solid	n_S	Density (kg/m^3)	Liquid	n_L	Density (kg/m^3)	Dynamic viscosity* (mPa s)	Phase	References
FEP	1.340	2150	Water	1.330	998	1 at 20 °C	Aq.	Hewitt et al. (1990) Amini and Hassan (2009) Amini and Hassan (2012) Hassan and Dominguez-Ontiveros (2008) Zadrazil et al. (2014) Zadrazil and Markides (2014) Satake et al. (2015)
THV	1.355	1970						Drobny (2006)
ETFE	1.403	1710						Ebnesajjad and Khaladkar (2005)
PVDF	1.420	1780						Ebnesajjad and Khaladkar (2005)
PVA	1.466–1471	1190	UCON oil 50-HB-5100 (polyglycol oil) 4 vol% Tetrabromohethane	1.467	1139	2460	Org.	Karnis et al. (1966)
			Cis-decalin Trans-decalin	1.471			Org.	Ottewill and Williams (1987)
PMMA	1.486–1.491	1180	Dow Corning 550 fluid (silicone oil) Dow Corning 200 fluid (silicone oil)				Org.	Johnston et al. (1975)
			84 wt% Dow Corning 550 (silicone oil) 16 wt% Dow Corning 556 (silicone oil)	1.490	1050	99.8	Org.	Stöhr et al. (2003)
			73 wt% Dow Corning 550 (silicone oil) 27 wt% Union Carbide L42 (silicone oil)	1.491	1060		Org.	Northrup et al. (1991)
			83 wt% Dow Corning 550 (silicone oil) 17 wt% Dow Corning 556 (silicone oil) Phenyl-tris(trimethylsilyloxy)silane	1.489–1.491	887	53.2	Org.	Peurrung et al. (1995) Rashidi et al. (1996) Braun et al. (1991)
			Dow Corning 550 (silicone oil)					Ng et al. (1978)
			Silicone fluid	1.490	988	40.35 at 25 °C	Org.	Prasad et al. (1991)
			Sodium salicylate Water	1.490			Aq.	Prasad et al. (1991)
			69.2 vol% Turpentine oil 30.8 vol% Tetralin	1.489	894	1.53	Org.	Tindal et al. (1988)
			68.2 vol% Turpentine oil 31.8 vol% Tetralin	1.489	894	1.46	Org.	Liu et al. (1989) Liu et al. (1990) Nouri et al. (1987)
			62.9 wt% Turpentine oil 37.1 wt% Tetralin	1.491	890	1.47	Org.	Kapoor and Acrivos (2006)
			2,2 Thiodiethanol Phosphate-buffered saline Glycerol	1.489				Zhu et al. (2016)

Table 1 continued

Solid	n_S	Density (kg/m^3)	Liquid	n_L	Density (kg/m^3)	Dynamic viscosity* (mPa s)	Phase	References
			Para-cymeme (p-cymeme)	1.489–1.490	853–860	0.5–1.195 0.741 at 25 °C	Org.	Frish and Webb (1981) Haam et al. (2000) Haam and Brodkey (2000) Hassan and Dominguez-Ontiveros (2008) Huang et al. (2008) Huang et al. (2009a) Huang et al. (2009b) Amini and Hassan (2012) Ni and Capart (2015)
			98.4–99.2 vol% Para-cymene 0.8–1.6 vol% Cinnamaldehyde					Fort et al. (2015)
			Ethyl and benzyl alcohol mixture					Hassan and Dominguez-Ontiveros (2008)
			Dibutylphthalate	1.490	1046–1118	15–20.71 16.583 at 25 °C	Org.	Ng et al. (1978) Frish and Webb (1981) Hendriks and Aviram (1982) Aziza and Wong (2003) Ovdat and Berkowitz (2006) Amini and Hassan (2012)
			14.07 wt% 1,1,2,2-Tetrabromoethane 35.66 wt% Polyalkylene glycol oil (UCON H-90000) 50.27 wt% Triton X100 0.1 wt% Tinuvin 328 (in TBE)	1.491	1182–1185	495 at 21.5 °C 495 at 23.2 °C		Abbott (1991) Graham (1991) Shauly et al. (1997)
			1,1,2,2-Tetrabromoethane polyalkylene glycol oil (UCON H-450) Triton X100 Tinuvin 328	1.491	1175			Averbakh et al. (1997)
			14.07 wt% 1,1,2,2-Tetrabromoethane 35.66 wt% Polyalkylene glycol oil (UCON HB-9500) 50.27 wt% Triton X100 0.1 wt% Tinuvin 328 (in TBE)	1.491	1182	103 at 23.25 °C		Abbott (1991)
			33.7 wt% Polyalkylene glycol oil 41.8 wt% Terpineol 24.4 wt% 1,1,2,2-Tetrabromohethane 0.1 wt% Tinuvin					Mondy et al. (1986) Majumdar et al. (1987)
			Shellflex 214 BG oil Kerosene			10 at 40 °C	Org.	Bovendeerd et al. (1987)
			62 wt% Polyalkylene glycol oil (UCON 50-HB-5100) 38 wt%1,1,2,2-Tetrabromoethane	1.491	1387 at 22 °C	2830 at 21.6 °C		Graham and Bird (1984)

Table 1 continued

Solid	n_S	Density (kg/m^3)	Liquid	n_L	Density (kg/m^3)	Dynamic viscosity* (mPa s)	Phase	References
			50% Triton X100 23% 1,6-Dibromohexane 13.5% UCON 75-H-90,000 oil 13.5% UCON 75-H-450 oil	1.487	1185–1190	480 at 20 °C		Lyon and Leal (1998a) Lyon and Leal (1998b)
			23 wt% UCON oil 75-H-90,000 77 wt% DER 331 liquid epoxy resin	1.489	1104	3000		Kaur and Leal (201)
			Hexadecane Sigma-Aldrich S150 microscope oil		890	25 at 25 °C	Org.	Lenoble et al. (2005)
			Triton X100	1.489	1070	240 at 23 °C		Jana (1995) Harrington et al. (2014)
			60–64 wt% Sodium iodide 36–40 wt% Water	1.485–1.500	1690–1840	1.382 at 28.9 °C 1.382 at 29 °C 1.47 at 26.7 °C 1.98	Aq.	Parker and Merati (1996) Uzol et al. (2002) Uzol et al. (2007) Soranna et al. (2008) Hassan and Dominguez-Ontiveros (2008) Yuki et al. (2008) Yuki et al. (2011) Mehta et al. (2007) Amatya and Longmire (2010) Tomac and Gregory (2014) Wu et al. (2009) Wu et al. (2011) Wu et al. (2012) Scholz et al. (2012)
			74 vol% Sodium iodide 21 vol% Glycerol 5 vol% Water	1.485	1700	5.4	Aq.	Zerai et al. (2005)
			79 vol% Saturated sodium iodide water solution 20 vol% Glycerol 1 vol% Water	1.490	1750	6.65 at 25 °C	Aq.	Baldwin et al. (1989) Baldwin et al. (1994)
			60 wt% Zinc iodide 40 wt% Water	1.487			Aq.	Hendriks and Aviram (1982)
			Ammonium thiocyanate Water				Aq.	Budwig et al. (1993) Egelhoff et al. (1999)
			37.5–41.1 wt% Ammonium thiocyanate 34.1–38.2 wt% Glycerol 24.3–24.8 wt% Water	1.485–1.488	1180–1210	4.99 at 22.5 °C 17.9	Aq.	Bailey and Yoda (2003) Jan et al. (1989)
			Potassium thiocyanate Water Glycerol	1.490	1230	2.2	Aq.	Jan et al. (1989)
			71 wt% Potassium thiocyanate 39 wt% Water	1.491		2.02 at 36 °C (mm^2/s)	Aq.	Gijsen et al. (1996) Budwig et al. (1993)
			85.5 vol% Diethylphthalate 14.5 vol% Ethanol	1.486		3.327 at 16.7 °C (mm^2/s)		Nguyen et al. (2004)

Table 1 continued

Solid	n_S	Density (kg/m^3)	Liquid	n_L	Density (kg/m^3)	Dynamic viscosity* (mPa s)	Phase	References
			40.67 wt% Glycerol 22.82 wt% Ethylene glycol 36.51 wt% Styrene glycol		1178	280		Leighton and Acrivos (1987)
			Glycerol Water					Agrawal et al. (1978)
			77.38 wt% Triton X100 13.39 wt% Zinc chloride 9.23 wt% Water	1.491	1172	3400 at 23 °C		Breedveld et al. (1998) Breedveld (2000) Breedveld et al. (2001) Breedveld et al. (2002)
			76 wt% Triton X100 16.2 wt% Zinc chloride 7.8 wt% Water	1.491	1180	16000 at 23 °C		Timberlake and Morris (2002)
			77.93 wt% Triton X100 9.01 wt% Zinc chloride 13.06 wt% Water		1172	3700 at 27 °C		Krishnan et al. (1996)
			Decalin Tetralin Cyclohexyl bromide					Gao and Kilfoil (2007) Chaudhuri et al. (2008)
			Decalin Tetralin Carbon tetrachloride					Kegel and van Blaaderen (2000)
			75.4 wt% Decalin 24.6 wt% Tetralin	1.510				Ackerson and Pusey (1988)
			65.6% Cyclohexyl bromide 34.4% Decalin			2.06 at 25 °C		Dibble et al. (2006)
			74 wt% Cyclohexyl bromide 26 wt% Decalin	1.490	1190			Wang et al. (2008)
			Cyclohexyl bromide Decalin Tetrabutyl-ammonium chloride					Kaufman and Weitz (2006)
			Sunflower oil	1.473		9.8 at 26 °C	Org.	Curran and Black (2004)
Nylon	1.514	1150	Pale 4 oil (oxidized castor oil) Tetrabromoethane	1.514	1138	1360	Org.	Karnis et al. (1966)
PS	1.590–1.600	1050	67.7 wt% 1-Methylnaphthalene 10.4 wt% 1-Chloronaphthalene 21.9 wt% Polyalkylene glycol	1.586–1.600	1052	124 at 20 °C	Org.	Koh et al. (1994)
			28 vol% 1-Methylnaphthalene 31 vol% 1-Chloronaphthalene 41 vol% Tetralin	1.590	1050	2.547	Org.	Cui and Adrian (1997)

* Temperature for viscosity is provided when stated; otherwise, it is assumed that this is at ambient laboratory conditions between 20 and 25 °C

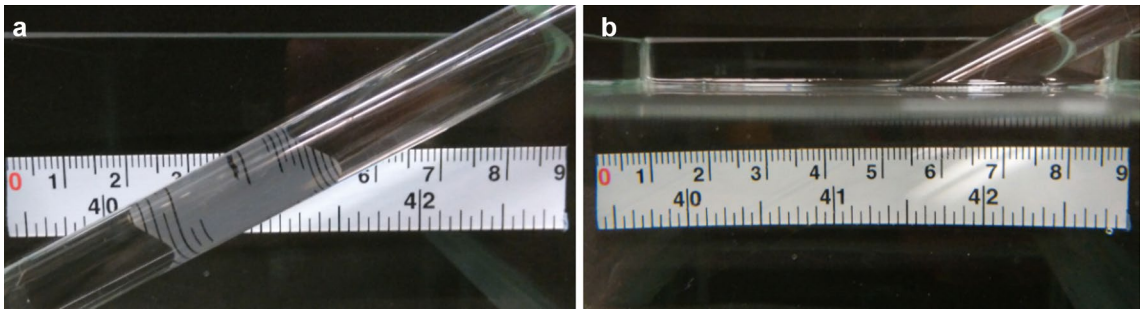

Fig. 7 Photographs of a PMMA rod in: **a** air, demonstrating large optical distortions; and **b** RIM Triton X100 liquid (RI = 1.489)

air–water contact angle of $\theta = 70°$ (Fort 1964). Our literature search has shown that Nylon has rarely been used in RIM experiments. Nevertheless, Nylon rods with a RI = 1.514 have been matched to a blend of Pale 4 oil (oxidized Castor oil) and tetrabromoethane to study optically dilute rod-shaped particle suspensions in Couette and Poiseuille flows (Karnis et al. 1966).

Polycarbonate (PC) is another common clear hard plastic with a RI of ≈ 1.580, a density of approximately 1210 kg/m^3, and an air–water contact angle of $\theta = 78°$ (Cho et al. 2003). Its relatively high RI means that combinations with aqueous solutions are rare, and as a result, no PC RIM experimental systems were found in the literature. Hendriks and Aviram (1982), however, showed that a zinc iodide (ZnI_2) solution could be created to match PC. Even so, Hirsch et al. (2015) found that distortions through polycarbonate windows lead to lower accuracy position measurements than with PMMA or glass, and that polycarbonate was also damaged by lower laser powers than PMMA and glass. As a result of these findings, Hirsch et al. (2015) recommended that polycarbonate should not be used for optical measurements.

Finally, referring to Table 1, PS is a transparent plastic with an RI between 1.590 and 1.600, a density of about 1050 kg/m^3 and an air–water contact angle of $\theta = 90°$ (Kondyurin et al. 2006). Of note is the fact that PS is vulnerable to a number of chemicals, such as cyclohexyl bromide and decalin (Dibble et al. 2006), and its use as a RIM solid in the literature is rare. However, one application example by Koh et al. (1994) had particles made from PS with divinylbenzene cross-linkage that were both density and RI (1.600) matched to a mixture of 1-methylnaphthalene, 1-chloronaphthalene, and polyalkylene glycol. It was suspected, however, that the PS particles slowly absorbed both the 1-methylnaphthalene and 1-chloronaphthalene causing the RIs of both the solids and liquids to vary over time (Koh et al. 1994). The relatively high RI of PS generally restricts the available fluid RIM options. Although no matching aqueous systems found in the literature, Hendriks and Aviram (1982) showed that a ZnI_2 aqueous solution can match PS.

A number of additional commercially available transparent or translucent solids of interest can be found on the market that have not yet been employed in RIM experiments to the best of the authors' knowledge. These include THV, ETFE, and PVDF, which are all hydrophobic fluoropolymers with RIs of 1.350, 1.403, and 1.420, densities of 1970, 1730, and 1780 kg/m^3, and air–water contact angles of $\theta = 99°$ (Begolo et al. 2011), $\theta = 99.2°$ (Akinci and Cobanoglu 2009), and $\theta = 94°$ (Saarinen et al. 2006), respectively. ETFE and PVDF are optically translucent rather than clear in the visible part of the electromagnetic spectrum (although slightly less clear than FEP), whereas THV is transparent. Both ETFE and PVDF are relatively stiff fluoropolymers allowing thin-walled tubes and other sections with adequate optical transparency to be constructed. As an example, the optical clarity of a 50-mm ID ETFE pipe with a 1-mm-thick wall can be seen in Fig. 8, while the optical clarity of a 14-mm ID PVDF pipe with a 0.7-mm-thick wall can be seen in Fig. 9. Similar to other fluoropolymers, like FEP, these materials have excellent chemical resistance. Of course, even with the mention of these plastics, this is not a complete list, especially since new materials are constantly emerging. Further plastic RIM options have been suggested by Wiederseiner et al. (2011), including polyetheretherketone (PEEK), polyethylene terephthalate (PET), polyvinylchloride (PVC), styrene/acrylonitrile copolymer (SAN), polychlorotrifluoroethylene (PCTFE), and polyformaldehyde (POM), with RIs of 1.650–1.770, 1.575, 1.540, 1.570, 1.435 and 1.410, respectively.

2.2 Silicone and urethane rubbers

Silicone rubbers are elastomers composed of a silicon-containing polymer. They typically have RIs in the range 1.410–1.440, while the air–water contact angle of PDMS silicone rubber is 108° (Duffy et al. 1998). The density of

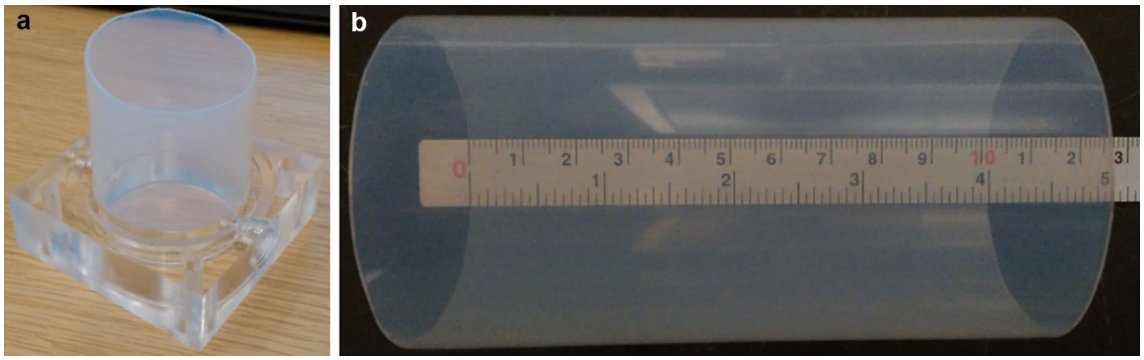

Fig. 8 Photographs of an ETFE pipe with a 50-mm ID and 1-mm wall thickness: **a** located within a PMMA flange; and **b** with an internal measurement tape

Fig. 9 Photograph of a PVDF pipe with a 14-mm ID and 0.7-mm wall thickness with an internal measurement tape

silicone rubber varies widely based on its exact composition; however, it is usually in the range of 1100–2300 kg/m^3. Flexibility makes silicone rubbers particularly useful for compliant models of flows through flexible structures or membrane-like tissues, e.g., in RIM models for blood-flow experiments and, as a result, have been frequently employed in such systems (Duncan et al. 1990; Perktold et al. 1997; Bale-Glickman et al. 2003; Burgmann et al. 2009; Shuib et al. 2010; Yousif et al. 2010; Gülan et al. 2012; Pielhop et al. 2012; Geoghegan et al. 2012; Im et al. 2013; Kefayati and Poepping 2013). Sylgard 184, manufactured by Dow Corning, has been identified as a silicone rubber of particularly interest (Duncan et al. 1990; Perktold et al. 1997; Hopkins et al. 2000; Yousif et al. 2010; Shuib et al. 2010; Buchmann et al. 2010, 2011; Geoghegan et al. 2012 and Kefayati and Poepping 2013). Although a common choice, Hopkins et al. (2000) cautioned that the effects of mixing and curing on Sylgard 184 can result in RI variations between models, and the care must, therefore, be taken in matching liquid RIs to individual models. It should be noted that silicone rubbers are known to absorb some liquids, including silicone oils and methlcyclohexane, and this can lead to significant swelling of the material (100% or more) while also potentially affecting the RI (Burdett et al. 1981). This is important in the practical deployment of these materials, as silicone oils are a close RI match for silicone rubbers but are unlikely to be suitable in most cases. An example of the use of silicone rubber is given in Im et al. (2013), where silicone rubber was RI matched to a glycerol solution to perform tomographic PIV measurements through a model of a nasal cavity.

Although rarely used, urethane is another transparent rubber that can be employed to study flows in compliant geometries. Le et al. (2013) matched urethane rubber with a RI of 1.490 to an aqueous solution of sodium iodide (NaI) and glycerol to study a model of an aneurysm. The different liquids identified as having been used in RIM experiments featuring rubbers are shown in Table 2.

2.3 Custom polymers, resins, and hydrogels

Optically clear resins have been developed with a very wide range of customized RIs (covering the range 1.31–1.60), and are currently available commercially from companies such as MY Polymers and Addison Clear Wave Inc. There are over 50 different types of optically clear resins on the market with varying composition, compatibility, and, of course, RI. Resins are frequently moulded into complex geometries, and can be found in optical equipment including lenses, optical adhesives, and fibre optics. The main advantage of using optically clear resins is that their RIs can be carefully tuned in a similar way to that of a mixture of liquids; however, the cost of these custom-made resins in relatively high may prove prohibitive, especially for large-scale experiments. In one successful implementation, Butscher et al. (2012) performed PIV measurements in a foam-like porous test section that was entirely made of the epoxy resin WaterShed XC 11122, which was RI matched to the liquid anisole at a RI of 1.515. In another example, Leis et al. (2005) examined the fluoropolymer–copolymer Nifion as RIM combination with water for studying biofilms. Importantly, Nifion is an atypical hydrophilic fluoropolymer with RI = 1.336–1.343 when water wetted.

Hydrogels comprise networks of polymer chains that contain large amounts of water (>90%), leading typically to RIs in the range 1.333–1.349. They have been used as

Table 2 List of rubber-based RIM systems

Solid	n_S	Density (kg/m^3)	Liquid	n_L	Density (kg/m^3)	Dynamic viscosity* (mPa s)	Phase	References
Silicone elastomer (silicone rubber) (PDMS)	1.410–1440	1100–2300	36.3 vol% Diethylphthalate 63.7 vol% Ethanol	1.410		1.818 at 23 °C		Miller et al. (2006)
			55.6 vol% Diethylphthalate 44.4 vol% Ethanol	1.440		3.327 at 16 °C (mm^2/s)		Nguyen et al. (2004)
			Methylcylohexane	1.422	772		Org.	Burdett et al. (1981)
			67.9 wt% Glycerol 32.1 wt% Water	1.422	1173	19.3	Aq.	Burdett et al. (1981)
			60.7 wt% Glycerol 39.3 wt% Water	1.406			Aq.	Burgmann et al. (2009)
			40 wt% Glycerol Water Sodium iodide	1.406			Aq.	Burgmann et al. (2009)
			59 vol% Glycerol 41 vol% Water	1.430		6.55 at 27.5 °C (mm^2/s)	Aq.	Hopkins et al. (2000)
			Glycerol Water				Aq.	Pielhop et al. (2012)
			60 wt% Glycerol 40 wt% Water	1.410	1160	5.4 at 37 °C	Aq.	Yagi et al. (2013)
			61 wt% Glycerol 39 wt% Water	1.417	1150	11.7 at 20 °C 12.7 at 20 °C	Aq.	Buchmann et al. (2010) Buchmann et al. (2011)
			61 wt% Glycerol 39 wt% Water	1.430	1140	10.6	Aq.	Geoghegan et al. (2012)
			59% Glycerol 41% Water	1.430		9.82 (mm^2/s)	Aq.	Im et al. (2013)
			36.94 wt% Glycerol 47.38 wt% Water 15.68 wt% Sodium iodide	1.410	1244	4.31 at 22.2 °C	Aq.	Yousif et al. (2010)
			37.1 wt% Glycerol 47.9 wt% Water 15.0 wt% Sodium chloride	1.410	1080	6.23 at 20 °C	Aq.	Shuib et al. (2010)
			36.84 wt% Glycerol 47.38 wt% Water 15.68 wt% Sodium iodide	1.414		4.31	Aq.	Kefayati and Poepping (2013)
			70 vol% Isopropyl alcohol 30 vol% Glycerol	1.410	930	13.95 at 25 °C		Bale-Glickman et al. (2003)
			Sodium thiocyanate Water	1.414		1.3 at 30 °C (mm^2/s)	Aq.	Duncan et al. (1990) Perktold et al. (1997)
Urethane rubber	1.490		20.8 wt% Glycerol 24.9 wt% Water 54.3 wt% Sodium iodide	1.490	1780	17.8	Aq.	Le et al. (2013)

* Temperature for viscosity is provided when stated; otherwise, it is assumed that this is at ambient laboratory conditions between 20 and 25 °C

Table 3 List of hydrogel, custom-polymer, and resin-based RIM systems

Solid	n_S	Density (kg/m^3)	Liquid	n_L	Density (kg/m^3)	Dynamic viscosity* (mPa s)	Phase	References
MEXFLON resin	1.330		Water	1.330			Aq.	Satake et al. (2015) Unno et al. (2016)
Hydrogel 0.4 wt% Agarose 99.6 wt% Water	1.333	1007	Water	1.330	998	1 at 20 °C	Aq.	Byron and Variano (2013)
Hydrogel 0.3 wt% Polyacrylamide 0.7 wt% Sodium acrylate Trace *N*,*N*-methylene-bis-acrylamide 99.0 wt% Water	1.333		Water	1.332			Aq.	Weitzman et al. (2014)
Nafion (fluoropolymer-copolymer)	1.336–1.343 (wet)		Water				Aq.	Leis et al. (2005)
Nafion (fluoroploymer-copolymer)	1.340		Water	1.330			Aq.	Downie et al. (2012)
Hydrogel 8.0 vol% Polyacrylamide/bis 0.5 vol% Ammonium persulphate 0.1 vol% Tetramethyl-ethylenediamine 91.4 vol% Water	1.349	1024	Water	1.330	998	1 at 20 °C	Aq.	Byron and Variano (2013)
Sumikagel		1010	Water		998	1 at 20 °C	Aq.	Kumar et al. (1993)
Hydrogel			Water		998	1 at 20 °C	Aq.	Kang et al. (2010)
Smooth-On Inc. Crystal Clear	1.498		65.0 wt% Sodium iodide 35.0 wt% Water	1.499			Aq.	Bai and Katz (2014)
Forecast3D UOPTIC 2	1.499		65.0 wt% Sodium iodide 35.0 wt% Water	1.499			Aq.	Bai and Katz (2014)
Renshape SL7870	1.508		66.8 wt% Sodium iodide 33.2 wt% Water	1.507			Aq.	Bai and Katz (2014)
Watershed XC 11122	1.512		Anisole	1.515	989	0.992 at 25 °C		Butscher et al. (2012)

* Temperature for viscosity is provided when stated; otherwise, it is assumed that this is at ambient laboratory conditions between 20 and 25 °C

particles in flows but are less likely to be suitable for use as rigid walls as they possess a degree of flexibility. The most common hydrogels include those based on polyacrylamide or agarose (Byron and Variano 2013). Weitzman et al. (2014) explored the use of copolymers of polyacrylamide and sodium acrylate in creating hydrogels that were RI matched to water while being readily available at low cost and easily moulded. In another successful application, hydrogel spheres and water were also RI matched by Kang et al. (2010) to perform visualization experiments showing the invasion drainage of porous media with density-matched immiscible liquids. The second liquid phase in these tests, an organic phase consisting of a mixture of soybean oil and carbon tetrachloride, was intentionally unmatched in RI, so that it could be easily identified and observed. The custom polymers, resins, and hydrogels identified in the literature as having been used in RIM experiments are listed in Table 3.

2.4 Glasses

Many glasses are readily available with a wide range of RIs (1.45–1.51). Glasses are of interest for RIM experiments as they are optically transparent and provide good chemical resistance, making them compatible with a variety of aqueous and organic fluids. Importantly, glasses can tolerate significantly higher laser powers than plastics before undergoing damage, which may be an important factor when higher illumination levels required (Hirsch et al. 2015), and they can also withstand higher stresses without significant deformation (e.g., due to pressure). On the other hand, glasses are not as easily machined and are typically more brittle than plastics. Glasses are typically hydrophilic and tend to be water wetted, e.g., in liquid–liquid water–oil flows. Common (clean) polished quartz and borosilicate glasses have contact angles in the range 10°–20° (Bowman 1998). Furthermore, glasses have a surface roughness of typically ~1 μm, which is the same as that of plastics pipes but smoother than metal pipes.

The RI of glass components varies slightly depending on their manufacturing process and composition. In the context of RIM experiments, RI variations should be established to ascertain their effect on measurement accuracy. Dijksman et al. (2012) found that different batches of glass beads had RIs that varied by up to 0.01. Similarly, the type of glass can affect optical accuracy. Hirsch et al. (2015) found that optical glass was, unsurprisingly, best suited for optical measurements but also that annealed-normal-glass had only slightly worse optical performance. Our RIM literature search revealed three common glass types: fused quartz; borosilicate; and soda-lime glass. RIM systems featuring these glasses can be found in Table 4, along with silica gel.

Fused quartz is high-purity silicon oxide (SiO_2) in amorphous (i.e., non-crystalline) form with a density of 2203 kg/m^3. It has both a lower coefficient of thermal expansion (5.5×10^{-7} K^{-1}) and a lower RI (1.450–1.460) compared to both borosilicate and soda-lime glasses, although its purity results in it being more expensive than these glasses. Fused quartz has featured in numerous RIM systems, including an RIM facility described by Stoots et al. (2001) for the purposes LDA flow studies around complex geometries for which the fused quartz observational sections of the facility were RI matched at 1.459 to a light mineral oil ("Penreco Drakeol #5"). McIlroy et al. (2010) then employed this flow system to study the turbulent flow in a gas-cooled reactor part using tomographic PIV.

Silica gel is a form of SiO_2 which is often in the form of granules or a porous material with a density of approximately 2210 kg/m^3 and an RI of 1.452. Silica gel is highly hydroscopic with a specific surface area of about 800 m^2/g. Once it becomes saturated with water, it can be regenerated by heating to 120 °C for 1 to 2 h. Silica gel has been used in a few RIM systems including that of Abbas and Crowe (1987) who used beads of silica gel that were RI matched to a mixture of chloroform and water to perform LDA measurements on homogenous slurry near transitional Reynolds numbers. Chloroform was selected in this study as it was considered reasonably priced, non-toxic, non-flammable, chemically stable, optically clear, and colourless.

Borosilicate glass, also known as Pyrex and Duran glass, is a laboratory glass with an RI in the range 1.470–1.474, a density of 2230 kg/m^3, and a thermal expansion coefficient of 3×10^{-6} K^{-1} which is generally lower than soda-lime glass but higher than fused quartz. The literature indicates that borosilicate glass is the second most common solid in RIM experiments behind PMMA. The wide use of borosilicate glass in RIM experiments has resulted in the identification of many liquid-phase matching substances (aqueous and organic). Similar to PMMA, borosilicate glass has been used for optical measurements in complex geometries, e.g., an aortic model (Walker et al. 1989) and flow through a porous medium (Cenedese and Viotti 1996). Reddy et al. (2013) created a solid–liquid fluidized bed for PIV measurements, where the solid bed was made from borosilicate glass spheres with a RI of 1.470 and the column was made from PMMA. A number of liquids were examined as matches to borosilicate spheres. A 55 wt% NaI solution (RI = 1.475) was RI matched but was considered too corrosive. A 42 wt% potassium thiocyanate (KSCN) solution (RI = 1.460) and a 45 wt% ammonium thiocyanate (NH_4SCN) solution (RI = 1.470) were also considered reasonable RI matches, but were also regarded too toxic and corrosive. Three further mixtures of benzene and turpentine (mixture RI = 1.470), turpentine and chloronaphthalene (RI = 1.465), and turpentine

and benzyl alcohol (RI = 1.470) were good RI matches for the borosilicate glass, but attacked the PMMA test section. A mixture of 68 wt% turpentine and 32 wt % tetralin (RI = 1.467) was found to RI match the borosilicate spheres, while also being compatible with the PMMA column. Finally, a light paraffin oil with an RI of 1.465 was also found to be a good RI match for borosilicate glass, whilst being compatible with the PMMA. This light paraffin oil was then added to adjust the viscosity of the 68 wt% turpentine and 32 wt% tetralin mixture used as the base experimental liquid.

Soda lime is the most common form of glass with a density of approximately 2520 kg/m^3. It is more brittle than both borosilicate and fused quartz, but has a lower cost. It is predominantly composed of silicon dioxide (SiO_2) along with other oxides including those of sodium (Na_2O), calcium (CaO), aluminium (Al_2O_3), potassium (K_2O), titanium (TiO_2), magnesium (MgO), iron (Fe_2O_3), sulphur (SO_3), and other impurities. The exact composition varies with the manufacturing process, which also affects the RI of the material between batches and suppliers. A search of the literature has shown that soda-lime glass typically has RI values between 1.50 and 1.52 due to this compositional variation. The relatively wide range of soda-lime glass RIs means that care must be taken when matching liquid(s) to solid components. Chen and Fan (1992) used two NaI solutions to match the RI of soda-lime and borosilicate glasses, in their study of 3-D flow structures in a solid–liquid–gas fluidized bed system. The soda-lime glass beads (RI = 1.500) of the fluidized bed were matched to a 60 wt% NaI solution, while the borosilicate cylindrical walls were enclosed in a box filled with a 55 wt% NaI solution that matched the RI of borosilicate (1.474). It is not clear why different glasses were selected for the beads and cylindrical walls, as the selection of the same glass would have led to a closer RI-matched system.

The lowest RI of the aforementioned glasses is that of fused quartz (RI = 1.450); nevertheless, the RI of calcium fluoride (CaF_2) glass is even lower at 1.434 (Malitson 1963). Given this RI, as well as its insolubility in water, CaF_2 appears as excellent RIM candidate for use in aqueous-based liquid–liquid systems; however, the authors have been unable to find examples of CaF_2 employed in this way in the literature. The mineral form of CaF_2, fluorite, is often fluorescent under ultraviolet light, and as a result, care should be taken when selecting the purity of the CaF_2 glass as well as the wavelength of any light-source/laser.

3 Multiphase flow systems

Optimal optical measurements (high-speed photography, LIF, LDV/PDA, and PIV/PTV) in liquid–liquid RIM systems require that the RIs of the two (or more) liquids and of the observational solids are closely matched. Liquid–liquid systems can be either miscible or immiscible. Miscible liquid–liquid RIM systems, which are considered single-phase flows here, are of interest, for instance when studying the mixing or multicomponent, density stratified flows (Hannoun 1985; Hannoun et al. 1988; De Silva and Fernando 1998; Daviero et al. 2001) or gravity-induced flows (McDougall 1979; Alahyari and Longmire 1994, 1997). The miscible liquids can be RI matched and the density can be tuned separately, for example, Alahyari and Longmire (1994) used two aqueous solutions (potassium dihydrogen phosphate (KH_2PO_4) and glycerol) to create a density difference of 4% in the RIM fluids. Similarly, beyond RI matching, it may be desirable to match also the viscosity of the liquids to set the Reynolds number or, alternatively, to introduce controlled viscosity variations that would be exhibited in processes such as the mixing of miscible systems. Nevertheless, these miscible liquid–liquid systems are not discussed any further, and we continue onto immiscible liquid–liquid systems.

Immiscible liquid–liquid systems are of interest in experiments that investigate complex multiphase flows consisting of two or more liquid phases. The majority of the relevant experiments reported in the literature have been performed in an environment where the liquid phases have been RI matched, but the observational solid phase has a different RI. While this is not ideal, in many cases, any curved solid surfaces (e.g., test-section walls) are static, thus making the optical distortions constant, so that they can be later corrected using the techniques described in the introduction. Consider the example of the liquid–liquid RIM system of Morgan et al. (2012), who applied planar LIF (PLIF) to horizontal liquid–liquid flows in a square test section. In this work, Exxsol D80 was RI matched at 1.444 to an 81.7 wt% glycerol solution. In Morgan et al. (2013, 2016), PLIF and PIV/PTV measurements were made using the same fluids but in a circular borosilicate glass pipe which had a RI of 1.474. The distortion caused by the mismatched solid RI was corrected for using a combination of a correction box and the graticule correction method.

In what follows, RIM systems are split into liquid–liquid (Sect. 3.1) and solid–liquid–liquid systems (Sect. 3.2).

3.1 Liquid–liquid systems

Transparent single-component immiscible liquid–liquid pairs, where one liquid was hydrophobic and the other hydrophilic, were experimentally studied by Smedley and Coles (1990). In all, they collated 121 compatible systems, of which 13 had an RI match of 0.001 or less, and a further 20 had RI differences of 0.005 or less. Given that all 121

Table 4 List of glass-based RIM systems including fused quartz, silica-gel, borosilicate, and soda-lime glass, as the solid phase

Solid	n_S	Density (kg/m^3)	Liquid	n_L	Density (kg/m^3)	Dynamic viscosity* (mPa s)	Phase	References
Fused quartz	1.450–1.460	2203	Tetraethylene glycol	1.459	1125	47.4 at 23.5 °C		Stephenson and Stewart (1986)
			Tetrahydropyran-2-methanol	1.458	1027	11.4 at 20 °C		Stephenson and Stewart (1986)
			90 vol% Cyclooctane 10 vol% Cyclooctene	1.458	834	2.42 at 20 °C		Stephenson and Stewart (1986)
			83.11 wt% Dimethylsulfoxide (DMSO) 16.89 wt% Water	1.462	1098	2.85 at 25.2 °C		Dietze et al. (2009)
			90.98 wt% Glycerol 9.02 wt% Water	1.462	1231	93.77 at 32.6 °C	Aq.	Dietze et al. (2009)
			Penreco Drakeol #5 (light mineral oil)	1.459			Org.	Stoots et al. (2001) McIlroy et al. (2010)
			70.3 vol% Diethylphthalate (DEP) 29.7 vol% Ethanol	1.459		3.499 at 23 °C		Miller et al. (2006)
			63 wt% Calcium chloride (dihydrate) 37 wt% Water	1.458		17 at 30 °C	Aq.	Amini and Hassan (2012)
			98 wt% Dow Corning 556 fluid (silicone oil) 2% wt% Dow Corning 200 fluid (silicone oil)	1.460	970	20.37	Org.	Stöhr et al. (2003)
			58 wt% Zinc chloride 42 wt% Water	1.460	1700	6.8	Aq.	Stöhr et al. (2003)
			60 wt% Soddard solvent* 40 wt% Mineral oil	1.445	812	4.1	Org.	Park et al. (1989)
			92 wt% Glycerol 8 wt% Water	1.456			Aq.	Park et al. (1989)
Silica gel	1.452		45 vol% Benzyl alcohol 55 vol% Ethyl alcohol	1.452	974	2.0 at 20 °C		Cui and Adrian (1997)
			Chloroform Water					Abbas and Crowe (1987)
			50 wt% Sodium iodide 50 wt% Water	1.443	1550	1.145 at 25 °C	Aq.	Wildman et al. (1992) Chen and Kadambi (1990) Chen and Kadambi (1995)
Borosilicate glass	1.470–1.474	2230	Trichloroethylene	1.474				Corino and Brodkey (1969)
			48.5 wt% Dow Corning 556 (silicone oil) 51.5 wt% Dow Corning 550 (silicone oil)	1.474		59 at 25 °C	Org.	Yarlagadda and Yoganathan (1989)

Table 4 continued

Solid	n_S	Density (kg/m^3)	Liquid	n_L	Density (kg/m^3)	Dynamic viscosity* (mPa s)	Phase	References
			68.9 vol% Dow Corning 556 (silicone oil) 31.1 vol% Dow Corning 550 (silicone oil)	1.474	1006	42.76	Org.	Wang and Khalili (2002)
			67.8 vol% Dow Corning 556 (silicone oil) 32.2 vol% Dow Corning 550 (silicone oil)	1.474	1006	42.76 at 23 °C	Org.	Goharzadeh et al. (2005)
			ESSO MARCOL 82 oil PRIMOL 352 oil	1.474			Org.	Saleh et al. (1992)
			55 wt% Sodium iodide 45 wt% Water	1.474			Aq.	Chen and Fan (1992) Chen et al. (1994)
			60 wt% Sodium iodide 40 wt% Water	1.470	1770	1.805	Aq.	Jacobs et al. (1988)
			58.5 wt% Sodium iodide 41.5 wt% Water	1.472			Aq.	Ghatage et al. (2014)
			54.5 wt% Sodium iodide 45.5 wt% Water	1.470			Aq.	Narrow et al. (2000)
			55 wt% Sodium iodide 45 wt% Water	1.475			Aq.	Reddy et al. (2013)
			81.1 vol% Diethylphthalate 18.9 vol% Ethanol	1.474		4.862 at 23 °C		Miller et al. (2006)
			Glycerol	1.470		954 at 23 °C	Aq.	Cenedese and Viotti (1996) Moroni and Cushman (2001)
			78.7 vol% Tetrechloroethylene 21.3 vol% Freon 113	1.471	1610	0.844		Varty (1984)
			Turpentine ethereal oil Xylene	1.470			Org.	Cenedese and Viotti (1996)
			Zinc chloride Water	1.470			Aq.	Cenedese and Viotti (1996)
			Decalin	1.470				Cenedese and Viotti (1996)
			Diesel oil mixture			4.3 at 20 °C (mm^2 s) 3.9 at 20 °C (mm^2 s)	Org.	Durst et al. (1995) Pashtrapanska et al. (2006)
			Ammonium thiocyanate Water				Aq.	Patil and Liburdy (2010) Patil and Liburdy (2012) Patil and Liburdy (2013)
			45 wt% Ammonium thiocyanate 55 wt% Water	1.470			Aq.	Reddy et al. (2013)
			Potassium thiocyanate Glycerol Water	1.482			Aq.	Walker et al. (1989)
			White Oil (FC 2012 W)	1.473			Org.	Schäfer et al. (1997)
			Paraffin oil light	1.465			Org.	Reddy et al. (2013)

Table 4 continued

Solid	n_S	Density (kg/m^3)	Liquid	n_L	Density (kg/m^3)	Dynamic viscosity* (mPa s)	Phase	References
			42 wt% Potassium thiocyanate 58 wt% Water	1.460			Aq.	Reddy et al. (2013)
			Turpentine Benzene	1.470				Reddy et al. (2013)
			Turpentine Chloronaphthalene	1.465				Reddy et al. (2013)
			Turpentine Benzyl alcohol	1.470				Reddy et al. (2013)
			68 wt % Turpentine 32 wt% Tetralin	1.467	915	1.20		Reddy et al. (2013)
			Turpentine Tetralin Paraffin oil light	1.465 –1.467	855–915	1.2–10.1		Reddy et al. (2013)
			66% Dipropylene glycol monomethyl ether 34% Diphenyal ether	1.474				Peterson et al. (1987)
			Oil (Pharma 5, DEA) light protective liquid (Eusolex, Merck)				Org.	Kohnen and Bohnet (2001)
Soda-lime glass	1.504–1.519	2520	Isopropyl alcohol Methylnaphthalene	1.504				Hassan and Dominguez-Ontiveros (2008)
			Heating oil (Diesel) Palationol					Durst and Loy (1985) Durst et al. (1988)
			Diethylphthalate	1.504	1180	12 at 20 °C		Hassan and Dominguez-Ontiveros (2008) Nguyen et al. (2004)
			28 wt% Tetralin 72 wt% TSF 451–1000 (silicone oil)	1.500	975	19.62	Org.	Mikami et al. (2001) Chen et al. (2005)
			Methyl benzoate	1.510				Zisselmar and Molerus (1979)
			Santicizer 278 (Monsanto)	1.510–1.519	1080–1090	912.6 at 24 °C 1300 at 22 °C		Ham and Homsy (1988) Nicolai and Guazzelli (1995) Nicolai et al. (1995) Nicolai et al. (1996)
			Tetralin Clear coal oil	1.513		2 at 20 °C	Org.	Zachos et al. (1996)
			60 wt% Sodium iodide 40 wt% Water	1.500			Aq.	Chen and Fan (1992)

* Temperature for viscosity is provided when stated; otherwise, it is assumed that this is at ambient laboratory conditions between 20 and 25 °C

Table 5 List of selected liquid–liquid systems

n_L	Phase	Material	Density (kg/m^3)	Dynamic viscosity* (mPa s)	Interfacial tension (mN/m)	References
1.322–1.335	Org.	57.9 wt% Perfluorohexane (FC-72) 39.1 wt% Hexane 3.0 wt% Perfluorohexyl hexane				Hibberd et al. (2007)
	Aq.	98.5 wt% Water 0.4 wt% Polyethylene glycol dodecyl ether 0.3 wt% Sodium azide 0.8 wt% Polyethylene oxide				
1.385	Org.	N-heptane	684	0.4 at 29 °C	31 at 29 °C	Pouplin et al. (2011)
	Aq.	43 vol% Glycerol 57 vol% Water	1102	3.2 at 29 °C		
1.391	Org.	Heptane	684	0.45 at 29 °C	31 at 29 °C	Conan et al. (2007)
		50 wt% Glycerol 50 wt% Water	1123	4.2 at 29 °C		
1.395 –1.436	Aq.	Water Caesium bromide 1,2-Propanedoil				Saksena et al. (2015)
	Org.	Silicone oil (5 cSt) Silicone oil (50 cSt) 1-Bromooctane				
1.382 –1.436	Aq.	Water Caesium bromide 1,2-Propanedoil				Cadillon et al. (2016)
	Org.	Silicone oil (1 cSt) Silicone oil (1000 cSt) 1-Bromooctane				
1.395	Org.	N-heptane	684	0.45 at 29 °C	31 at 29 °C	Augier et al. (2003) Augier et al. (2007)
	Aq.	50 wt% Glycerol 50 wt% Water	1180	6 at 29 °C		
1.396	Org.	62.4 wt% Freon 37.6 wt% Octanol				Budwig (1994)
	Aq.	37.8 wt% Sucrose 62.2 wt% Water				
1.399–1.403	Org.	Silicone oil (6 cSt)	925	5.4@ 20 °C		Ninomiya and Yasuda (2006)
	Org.	Silicone oil (20 cSt)	950	18.32 at 20 °C		
	Aq.	50 wt% Glycerol 50 wt% Water	1130	6.7 at 20 °C		
1.400	Org.	Dow Corning 200 (20 cSt silicone oil)	949	19	29.1	Mohamed-Kassim and Longmire (2003) Mohamed-Kassim and Longmire (2004)
	Aq.	45 vol% Glycerol 55 vol% Water	1128	6.3		
1.401	Org.	Wacker AK 100 silicone oil		96 at 25 °C		Kollhoff et al. (2015)
	Aq.	20.19 wt% Sodium chloride 18.75 wt% Sucrose 61.06 wt% DI water		3.7 at 25 °C		
1.399–1.401	Org.	Silicone oil (11 mPa s)	940	1.4		Svensson and Rasmuson (2004) Svensson and Rasmuson (2006)
	Aq.	30 wt% Sodium iodide 70 wt% Water	1340	11		
1.401	Org	Silicone oil (50 cSt)	960	48	29.1–29.5	Bordoloi and Longmire (2012) Longmire and Bordoloi (2015)
	Aq.	48 vol% Glycerol 52 vol% Water	1130	6.7–7		
	Org	Silicone oil (20 cSt)	950	19	25.7	Longmire and Bordoloi (2015)
	Aq.	48 vol% Glycerol 52 vol% Water	1130	7		

Table 5 continued

n_L	Phase	Material	Density (kg/m^3)	Dynamic viscosity* (mPa s)	Interfacial tension (mN/m)	References
1.401	Org.	Dow Corning 200 (50 cSt silicone oil)	960	48	29.1–29.5	Mohamed-Kassim and Longmire (2003)
	Aq.	46 vol% Glycerol 54 vol% Water	1131	6.7		Mohamed-Kassim and Longmire (2004) Kim and Longmire (2009) Ortiz-Dueñas et al. (2010)
1.394–1.407	Org.	Dow Corning 200 (5 cSt silicone oil)	970	4.85	29.5	Longmire et al. (2001)
	Org.	Dow Corning 200 (50 cSt silicone oil)	960	48		
	Aq.	56 wt% Glycerol 44 wt% Water	1140	8.33		
1.431–1.432	Org.	Diethyl pimelate	994	4.0 at 20 °C		Smedley and Coles (1990)
	Aq.	Ethylene glycol	1109	19.9 at 20 °C		
1.431–1.432	Org.	Dipropyl adipate	979			Smedley and Coles (1990)
	Aq.	1,2-Propanedoil	1036	56.0 at 20 °C		
1.431–1.432	Org.	Ethyl laurate	862	3.4 at 20 °C		Smedley and Coles (1990)
	Aq.	1,2-Propanedoil	1036	56.0 at 20 °C		
1.431–1.432	Org.	Dipropyl adipate	979			Smedley and Coles (1990)
	Aq.	Ethylene glycol	1109	19.9 at 20 °C		
1.431–1.432	Org.	Ethyl laurate	862	3.4 at 20 °C		Smedley and Coles (1990)
	Aq.	Ethylene glycol	1109	19.9 at 20 °C		
1.432	Org.	Methyl laurate	870	3.1 at 20 °C		Smedley and Coles (1990)
	Aq.	1,2-Propanedoil	1036	56.0 at 20 °C		
1.432	Org.	Methyl laurate	870	3.1 at 20 °C		Smedley and Coles (1990)
	Aq.	Ethylene glycol	1109	19.9 at 20 °C		
1.432	Org.	Glycerol tripropanoate	1098	14.3 at 20 °C		Smedley and Coles (1990)
	Aq.	Ethylene glycol	1109	19.9 at 20 °C		
1.438	Org.	Exxsol D80	803	1.62 at 25 °C	19 at 20 °C	Liu (2005)
	Aq.	39 wt% Calcium chloride 61 wt% Water	1442	11.84 at 25 °C		Liu et al. (2006a) Liu et al. (2006b)
	Org.	Silicone oil (0.65 cSt)		0.65 (mm^2 s)	43	Berard et al. (2013)
	Org.	Silicone oil (5 cSt)		5 (mm^2 s)		
	Org.	Silicone oil (20 cSt)		20 (mm^2 s)		
	Aq.	Glycerol Water				
1.440–1.441	Org.	2-Bromopentane	1208			Smedley and Coles (1990)
	Aq.	1,3-Propanedoil	1060	46.6 at 20 °C		
1.440	Org.	1-Bromobutane	1276	0.64 at 20 °C		Smedley and Coles (1990)
	Aq.	1,3-Propanedoil	1060	46.6 at 20 °C		
1.444	Org.	Exxsol D80	803	1.9 at 20 °C	25	Morgan et al. (2012)
	Aq.	81.7 wt% Glycerol 18.3 wt% Water	1213	82.3 at 20 °C		Morgan et al. (2013) Morgan et al. (2016)
1.446	Org.	Shell Macron EDM110 oil	800	3.0 at 20 °C	45	Ravelet et al. (2007)
	Aq.	510 g/L Sodium iodide water solution	1500	2.0 at 20 °C		
1.447	Org.	Bis(2-ethylhexyl) adipate	922	13.3 at 20 °C		Smedley and Coles (1990)
	Aq.	Formamide	1133	3.85 at 20 °C		
1.447–1.448	Org.	1-Bromohexane	1174	1.1 at 20 °C		Smedley and Coles (1990)
	Aq.	Diethylene glycol	1116	35.7 at 20 °C		
1.448–1.449	Org.	1-Bromohexane	1174	1.1 at 20 °C		Smedley and Coles (1990)
	Aq.	1,5-Pentanediol	992	128.1 at 20 °C		

* Temperature for viscosity is provided when stated; otherwise, it is assumed that this is at ambient laboratory conditions between 20 and 25 °C

systems were single component and, therefore, not tuned in RI, it seems likely that many of these systems could be significantly improved upon through blending or additives (see Sect. 4). The 13 closest RIM pairs of Smedley and Coles (1990) are included in Table 5. It is worth noting that none of RIM systems in Smedley and Coles (1990) involve the commonly used RIM fluids of water, glycerol, or silicone oil. These liquids can, however, be found in many other liquid–liquid RIM systems included in Table 5. The RIs of the matched liquid–liquid systems span the range from 1.322 to 1.460, with the majority of actual experimental flow systems being near a value of 1.40.

3.2 Solid–liquid–liquid systems

Our review of the literature has shown that RIM systems have been used predominantly for experiments featuring solid–liquid systems, and that while liquid–liquid RIM systems are common, full three-phase solid–liquid–liquid RIM systems are rare, with only a few cases reported in the literature. In one such effort, Burdett et al. (1981) investigated a solid–liquid–liquid RIM system for studying dispersed flows, holdup, and axial mixing in packed extraction columns. The matching of liquid–liquid systems with PMMA was considered, but this was disregarded as the aqueous phase consisted of concentrated salt solutions that were deemed too corrosive. Glycerol solutions were also considered, but the viscosity of these solutions was considered too high when over 70 wt% of glycerol was added, limiting the maximum achievable RI to about 1.430. A number of solids below this limit were then considered including polytetrafluoroethylene (PTFE), polyformaldehyde (PFA), polychlorotrifluoroethylene (PCTFE), and silicone rubber, with respective RIs of 1.380, 1.410, 1.430, and 1.420. Silicone rubber was ultimately selected as this was fairly transparent and chemically inert. The silicone rubber was then RI matched to two immiscible fluids, where the aqueous phase was a 67.9 wt% glycerol solution and the organic phase was methylcyclohexane. In another study, by Stöhr et al. (2003), two-phase liquid flows through porous media were investigated using PLIF and a fully matched RIM system. The porous medium consisted of fused quartz matched to two immiscible fluid combinations. The first immiscible fluid was a mixture of silicone oils (98 wt% Dow Corning 556 fluid and 2 wt% Dow Corning 200 fluid), while the second fluid was an aqueous solution of 58 wt% zinc chloride ($ZnCl_2$).

Given that the majority of liquid–liquid RIM systems reported in Tables 5 and 6 have RIs around 1.40, it is surprising that ETFE (1.403) has not been reported in the literature as a matching solid for these systems. A compatible non-hazardous and readily available solid–liquid–liquid RIM system can be created using ETFE with a silicone oil and an approximately 50 wt% glycerol solution. Since silicone oils have a wide range of viscosities with RIs near 1.400, this system allows for considerable tuning of the liquid viscosity ratios. Figure 10a shows an ETFE pipe in air, while Fig. 10b shows the same ETFE pipe matched to a stratified colourless liquid–liquid system of a 10^{-5} m^2/s silicone oil (on top) and a 51 wt% glycerol solution (on the bottom). Viewed face-on, the interface between the two liquids is barely visible in Fig. 10b; however, the top silicone oil layer light undergoes significantly more visible colour splitting along the length of the scale.

4 Refractive index, density, and viscosity tuning

While some liquids are naturally close optical matches to other liquids or solids, the RI of liquids in general can to be tuned to obtain a required RI matching degree by mixing miscible liquids or adding soluble solids. This practice also requires the ability to predict the RI of the resulting liquid mixtures or solutions. The RI of such mixtures can be predicted by numerous relations, with the most common of these listed below; here: n is the RI, φ is the volume fraction and the subscripts indicate the component.

A simple prediction of the RI of a multicomponent liquid can be made using the empirical Arago-Biot (AB) equation (Arago and Biot 1806; Reis et al. 2010), which is based on linear volumetric additivity for each component in the mixture:

$$n = \sum_i \varphi_i n_i, \tag{4}$$

and is similar to the empirical Gladstone–Dale (GD) equation (Gladstone and Dale 1863; Sharma et al. 2007):

$$n - 1 = \sum_i \varphi_i (n - 1). \tag{5}$$

Another empirical relation is the Lichtenecker (L) or Lichtenecker–Rother equation (Lichtenecker 1926; Lichtenecker and Rother 1931; Heller 1945) which, as Simpkin (2010) showed, in fact, has a theoretical basis and can be derived from Maxwell's equations:

$$\ln n = \sum_i \varphi_i \ln n_i, \tag{6}$$

while relatively common Newton (N) equation (Newton 1704; Kurtz and Ward 1936; Reis et al. 2010) also has a theoretical foundation:

$$n^2 = \sum_i \varphi_i n_i^2. \tag{7}$$

Table 6 List of selected solid–liquid–liquid RIM systems

n	Phase	Material	Density (kg/m^3)	Dynamic viscosity* (mPa s)	Interfacial tension (mN/m)	References
1.422	Sol.	Silicone rubber			n/a	Burdett et al. (1981)
	Org.	Methylcyclohexane	772		41.3	
	Aq.	67.9 wt% Glycerol 32.1 wt% Water	1173	19.3		
1.460	Sol.	Fused quartz	2200	n/a	n/a	Stöhr et al. (2003)
	Org.	98 wt% Dow Corning 556 fluid (silicone oil) 2 wt% Dow Corning 200 fluid (silicone oil)	970	21		
	Aq.	58 wt% Zinc chloride 42 wt% Water	1700	4		

* Temperature for viscosity is provided when stated; otherwise, it is assumed that this is at ambient laboratory conditions between 20 and 25 °C

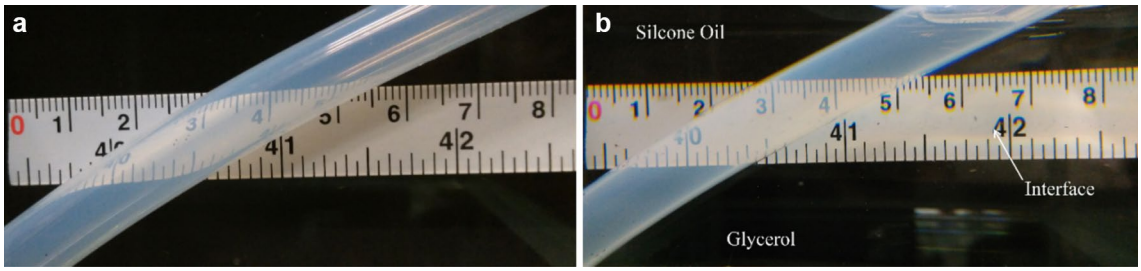

Fig. 10 ETFE (RI = 1.403) pipe in: **a** air, demonstrating large optical distortions; and **b** stratified layers of refractive-index-matched liquids (RI = 1.399) comprising a silicone oil on top and a 51 wt% glycerol solution on the bottom

Proceeding now to more complex models, the more involved theoretical Oster (O) equation (Oster 1948; Sharma et al. 2007) is:

$$\frac{\left(n^2-1\right)\left(2n^2+1\right)}{n^2}=\sum_i \varphi_i \frac{\left(n_i^2-1\right)\left(2n_i^2+1\right)}{n_i^2}, \tag{8}$$

while the Lorentz–Lorenz (LL) equation, which is also a theoretical model that is based on material polarizability (Lorentz 1906; Pacák and Kodejš 1988), has a similar form:

$$\frac{n^2-1}{\left(n^2+2\right)}=\sum_i \varphi_i \left(\frac{n_i^2-1}{n_i^2+2}\right), \tag{9}$$

as does the empirical Eykman (E) equation (Eykman 1895; Dreisbach 1948; Sharma et al. 2007):

$$\frac{n-1}{(n+0.4)}=\sum_i \varphi_i \left(\frac{n_i^2-1}{n_i+0.4}\right). \tag{10}$$

Furthermore, the RIs of binary mixtures can be calculated by the Eyring–John (EJ) equation (Eyring and Jhon 1969):

$$n=n_1\varphi_1^2+2(n_1n_2)^{1/2}\varphi_1\varphi_2+n_2\varphi_2^2, \tag{11}$$

and for dilute binary mixtures, where component "2" is denoted here as the dilute component, the RI can be calculated using the theoretical Wiener (W) equation (Wiener 1910; Heller 1945; Wiederseiner et al. 2011):

$$\frac{n-1}{n^2+2n_1^2}=\varphi_2\frac{n_2^2-n_1^2}{n_2^2-2n_1^2}, \tag{12}$$

or using the theoretically derived Heller (H) equation (Heller 1945; Mehra 2003):

$$\frac{n-n_1}{n_1}=\frac{3}{2}\varphi_2\frac{n_2^2-n_1^2}{n_2^2-2n_1^2}. \tag{13}$$

In all the above expressions, the volume fraction of a component "i", φ_i, is defined using Eq. 14, where V and x are molar volumes and molar fractions, respectively (Sharma et al. 2007):

$$\varphi_i=\frac{x_iV_i}{\sum_j x_jV_j}. \tag{14}$$

The theory behind the RI of liquid mixtures is discussed by Reis et al. (2010), who explains that differences between the AB and N equations, which are amongst the simplest of the above relations, stem from the rigorous definitions of RI before and after mixing, respectively. In trying to establish which relation appears better suited for the prediction of the RI of liquid mixtures, we examined comparisons performed by a number of authors. In one such effort that focussed on binary mixtures, Tasić et al. (1992) compared the AB, GD, LL, W, and H equations concluding that LL predictions agreed very well with RI measurements, whereas the AB relation was found to be the poorest predictor. Mehra (2003) tested the GD, LL, W, and H equations in relation to binary mixtures of hexadecane and heptadecane with a series of alcohols, and concluded that the GD and W equations did not perform as well as the LL or H equations. The authors also noted that the GD equation gave the same results as the W equation in very dilute mixtures but that neither worked well at higher concentrations. In their extensive study, Sharma et al. (2007) compared the AB, GD, N, O, LL, E, EJ, W, and H equations, and considered the H equation to be most accurate for their specific binary test mixtures of eucalyptol with hydrocarbons. The authors noted small deviations between the AB and GD predictions, and reported that the W equation exhibited larger deviations from experimental RI values than the E, EJ, and H equations. In another comprehensive study involving multiple empirical and theoretical relations, Mandava et al. (2015) compared the AB, GD, N, O, LL, E, EJ, W, and H equations and found that the O relation was the worst performing for their mixtures, while the N equation performed the best. Isehunwa et al. (2015) compared predictions of the RIs of selected binary mixtures from the AB, GD, LL, W and H equations, and found that their own modified AB equation had the widest temperature applicability.

From the above variability over the best performing relation(s), but also a large number of similar studies in the literature, it is clear that these equations should be treated as a guide and that RI should be measured whenever possible, but also that it is a great challenge to identify one relation that can be generally accepted as being best with different relations performing better with different liquid phases and their relative mixture concentrations. Nevertheless, Mehra (2003) states that the most frequently used equation is LL equation, and although in the above comparisons only, Tasić et al. (1992) and Mehra (2003) found LL to be the most accurate approach, none found that it was the worst performing. Based on this observation, the present authors consider that the LL equation appears to be the most promising, at least as a good starting point, for the purposes of RI tuning.

Importantly, combining three or more liquids or additives allows for the matching or tuning of parameters over and above the RI, i.e., density, viscosity, surface, and interfacial tensions, for the purpose of flow similarity. Density tuning is desirable when gravitational effects need to be considered in both solid–liquid and liquid–liquid systems and is particularly important when trying to establish neutrally buoyant solids (Bailey and Yoda 2003). Viscosity tuning is important when trying to obtain direct matches to actual liquids or when matching Reynolds numbers. Likewise, the interfacial tension can be important in liquid–liquid systems when investigating interfacial phenomena (droplet breakup, atomization, etc.). The prediction of density, viscosity, and surface tension is beyond the scope of this paper, so the reader is referred to Polling et al. (2001) which is an excellent reference source covering a range of methods for estimating these properties for a wide range of liquids, and their mixtures. Combinations can also allow RI tuning at two wavelengths simultaneously, for example, the wavelengths of laser emission and dye fluorescence (Saksena et al. 2015).

Furthermore, many physio/biological, petrochemical, and other flows involve complex non-Newtonian fluids for which it is often desirable to tune additional properties in RIM experiments, such as the fluid rheology, to achieve dynamic similarity with flows of interest. For example, the shear thinning and viscoelastic behaviour of blood is often modelled by adding xanthan gum, and the further addition of NaI or sodium thiocyanate (NaSCN) can be used to reduce the viscosity of the resultant xanthan gum mixtures (Najjari et al. 2016).

Tuning for dynamic similarity in two-phase flow systems where (Newtonian) viscosity, density, and interfacial tension are important can be achieved by satisfying Eqs. 15, 16, 17 for the liquid phases of interest A and B, and the surrogate/model liquids SA and SB (Saksena et al. 2015). Equations 15 and 16 equate the density and viscosity ratios of the surrogate and actual liquids, while Eq. 17 is required for matching dimensionless numbers concerning interfacial tension including the Weber number, Bond number, capillary number, Eötvös number, and Ohnesorge number:

$$\frac{\rho_{SA}}{\rho_{SB}} = \frac{\rho_A}{\rho_B}; \tag{15}$$

$$\frac{\mu_{SA}}{\mu_{SB}} = \frac{\mu_A}{\mu_B}; \tag{16}$$

$$\frac{\sigma^3_{SA:SB}\rho_{SA}}{\mu^4_{SA}} = \frac{\sigma^3_{A:B}\rho_A}{\mu^4_A}. \tag{17}$$

A highly tuneable liquid–liquid RIM system with a RI covering the range from 1.395 and 1.436 was created by Saksena et al. (2015). This system simultaneously allowed control over RI, viscosity, and density, as well as a potential

4th parameter. This flexibility was achieved through having two-liquid-mixture phases: an aqueous solution containing 1,2-propanedoil and caesium bromide (CsBr), and an organic phase comprising a light (5×10^{-6} m^2/s) and heavy (5×10^{-5} m^2/s) silicone oil blended with 1-bromooctane. The system was extended for wider viscosity and density ratios by Cadillon et al. (2016) by replacing the silicone oils with ones with even larger viscosity differences (1×10^{-6} m^2/s and 5×10^{-3} m^2/s) to obtain a system with an RI in the range 1.382–1.436.

An experimental system will typically define a working temperature range. Temperature variations can, however, give rise to RI variations, meaning that RI tuning may be required even for what superficially appears to be a RIM system. In one example, Fort et al. (2015) demonstrated that para-cymene closely matched PMMA at 291.7 K, but noted that a cooling system may be required if heat sources, such as pumps, exist within a flow loop. It was, therefore, suggested that para-cymene's RI could be tuned through adding a small amount of cinnamaldehyde with an RI of 1.562 to allow RI matching with PMMA at higher temperatures.

The present authors measured the RI of two liquids over a range of temperatures: (i) polydimethylsiloxane silicone oil with a kinematic viscosity 10^{-5} m^2/s; and (ii) four RIM glycerol solutions, and the results are plotted in Fig. 11. The two fluid types have different RI temperature gradients, which can cause matched systems to diverge with temperature. A change of about 4 °C corresponds to an RI change of the same magnitude as that due to a 1 wt% difference in glycerol concentration. These variations can, in principle, be limited using ternary systems to simultaneously tune the RI and the RI temperature gradients of a two-liquid system; however, no system has been found in the literature implementing this RI temperature gradient matching technique.

The effect on the RI of different glycerol solution concentrations over the entire range of mole fractions for temperatures between 25 and 60 °C is reported in a comprehensive study by Leron et al. (2012), and associated results are plotted here in Fig. 12. This figure shows that the temperature change of 35 °C corresponds to a change in RI of up to ~0.01.

The following sections describe organic and aqueous liquids, as well as salts found in experiments featuring RIM systems.

4.1 Organic liquids

A wide range of organic liquids have been employed in RIM systems, including pure hydrocarbons, hydrocarbon mixtures, mineral or silicone oils, fluorocarbons, etc. A selection of such fluids is listed in Table 7, covering an RI range from 1.251 to 1.631. The table forms a guide for the

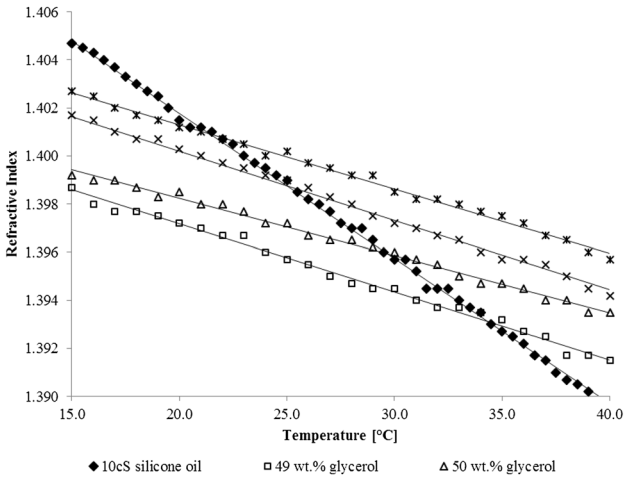

Fig. 11 RI variation with temperature for a silicone oil with viscosity 10^{-5} m^2/s and a range of closely RIM glycerol solutions

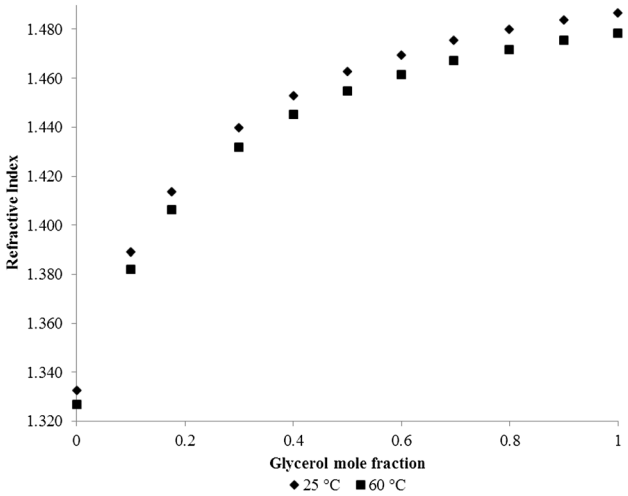

Fig. 12 RI variation with temperature between 25 and 60 °C for a full range of glycerol solutions; data from Leron et al. (2012)

selection of potential components for tuning organic mixtures. For instance, high RI organic chemicals like tetralin (RI = 1.541) can be added to increase the RI of another organic phase, while similarly, low RI liquids like tetradecafluorohexane can be added to lower the RI. Table 7 also provides water solubility as well as PMMA compatibility information that has been obtained principally via supplier datasheets and should be regarded as approximate guidance only.

In general, the RI of hydrocarbons within a given chemical class generally increases with the size/weight or complexity of their chemical structure. Fluorocarbons have relatively low RIs, and importantly, many fluorocarbons have RIs that are lower than water. This proximity in their RI to that of water makes fluorocarbon-based blends suitable as

Table 7 List of organic liquids previously in RIM experiments, with their RI, surface tension, dynamic viscosity, and density

Liquid	n_S	Density (kg/m^3)	Dynamic viscosity* (mPa s)	Surface tension (mN/m)	Water solubility	PMMA compatibility	References
Tetradecafluorohexane	1.251	1680	0.635 at 25 °C	12.23 at 25 °C	Immiscible		Hibberd et al. (2007)
Freon-113	1.356				Poor		Varty (1984)
N-hexane	1.375–1.381	659	0.3 at 25 °C	18.4 at 20 °C	Immiscible	Good	Hibberd et al. (2007) Blanchette and Bigioni (2009)
Isopropyl alcohol	1.378	785	2.038 at 25 °C	20.93 at 25 °C	Miscible	Poor	Hassan and Dominguez-Ontiveros (2008) Hayes (2015)
Heptane	1.395	684	0.45 at 29 °C	19.66 at 25 °C	Immiscible	Poor	Augier et al. (2003) Hayes (2015)
Dow Corning 200 (silicone oil)	1.375–1.404	978	0.65–1,000,000 at 25 °C	19.7–21.6	Immiscible	Good	Dow Corning datasheets
Exxsol D60	1.434	785	1.64 at 15 °C		Immiscible	Good	Amundsen (2011)
Soddard solvent	1.438	789			Immiscible	Poor	Carpenter et al. (1975)
Chloroform	1.441	1472	0.537 at 25 °C	26.67	Slightly	Poor	Bhatia et al. (2009) Hayes (2015)
Exxsol D80	1.444	796	2.3 at 21 °C		Immiscible	Good	Morgan et al. (2012)
Carbon tetrachloride	1.453	1580	0.9	45	Immiscible	Poor	Tidhar et al. (1986) Rheims et al. (1997)
UCON H-450 (polyalkylene glycol oil)	1.457	1084	120		Miscible	Poor	Averbakh et al. (1997)
Exxsol D140	1.459	828	6 at 25 °C	27.6	Immiscible	Good	Lovick and Angeli (2004)
Dow Corning 556 (silicone oil)	1.460	980	22.5 at 23 °C		Immiscible	Good	Goharzadeh et al. (2005)
UCON 75-H-90000 (polyalkylene glycol oil)	1.464	1094	51100 at 20 °C		Miscible	Poor	Koh et al. (1994) Kaur and Leal (2010)
Turpentine	1.464	850	1.43		Immiscible	Good	Kapoor and Acrivos (2006)
Decalin (decahydronaphthalene)	1.470	897	2.2 at 25 °C		Immiscible	Poor	Miller et al. (2006) Hayes (2015)
Triton X100	1.487	1055	280 at 28 °C		Miscible	Poor	Averbakh et al. (1997)

Table 7 continued

Liquid	n_S	Density (kg/m^3)	Dynamic viscosity* (mPa s)	Surface tension (mN/m)	Water solubility	PMMA compatibility	References
Para-cymeme (p–cymeme)	1.489	855	1.023		Immiscible		Ni and Capart (2015)
Dibutylphthalate (DBP)	1.49	1049	16.6 at 25 °C		Immiscible	Poor	Aziza and Wong (2003) Hayes (2015)
Xylene	1.493	860	0.6 at 26 °C	29.76 at 25 °C	Immiscible	Poor	Richards and Scheele (1985) Hayes (2015)
Dow Corning 550 (silicone oil)	1.494	1068	125 at 23 °C	24.5	Immiscible	Good	Goharzadeh et al. (2005) Stöhr et al. (2003)
Cyclohexyl bromide	1.495				Immiscible		Dijksman et al. (2012)
Diethylphthalate (DEP)	1.504	1180	12		Immiscible	Poor	Nguyen et al. (2004)
Tetrachloroethylene	1.504	1615	0.861 at 25 °C		Poor	Poor	Baragi et al. (2005)
Anisole	1.515	989	0.992 at 25 °C	35.10	Immiscible		Baragi et al. (2005) Hayes (2015)
Methyl salicylate	1.526	1180	4.09	35	Poor	Poor	Nguyen et al. (2004) Merrington and Richardson (1947)
Dow Corning 710 (silicone oil)	1.533	1110	500	28.5	Immiscible	Good	Stöhr et al. (2003)
Benzyl alcohol	1.540	1045	2 at 20 °C	27.89 at 75 °C	Slightly	Poor	Cui and Adrian (1997) Hayes (2015)
Tetralin (tetrahydronaphthalene)	1.546	967–970	2.2 at 20 °C	33.17 at 25 °C	Immiscible		Cui and Adrian (1997) Hayes (2015)
Methylnaphthalene	1.616	1017	3.29 at 20 °C		Immiscible	Poor	Koh et al. (1994)
Tetrabromoethane (TBE)	1.624	2943	1		Poor		Averbakh et al. (1997)
Chloronaphthalene	1.631	1191	3.42 at 20 °C		Poor		Koh et al. (1994)

* Temperature for viscosity is provided when stated; otherwise, it is assumed that this is at ambient laboratory conditions between 20 and 25 °C

organic liquid candidates for solid–liquid–liquid RIM systems with water and FEP as the aqueous and solid phases, respectively. Although sourcing fluorocarbons in both reasonable quantities and cost may, in some cases, prove difficult, especially for large system (Saksena et al. 2015), Hibberd et al. (2007) reported using tetradecafluorohexane and n-hexane with RIs of 1.251 and 1.378, respectively, to prepare a water-based RIM emulsion. Of importance in this case is the flammability and relatively low boiling points of tetradecafluorohexane (<61 °C) and *n*-hexane (<69 °C), which introduce the need to apply caution when handing these fluids outside of controlled, closed environments. Longer chain fluorocarbons are potentially even more suitable for experimental systems, e.g., Vitreon (perfluoroperhydrophenanthrene) has RI = 1.335 (close to water) and is both non-toxic and non-volatile (Georgalas et al. 2011). A combination of FEP, water and perfluoroperhydrophenanthrene, therefore, appears to be a promising candidate for a water-based RI matched liquid-liquid system.

Silicone oils are another group of organic liquids worth mentioning. In general, they are non-toxic and have wide ranges of both RIs and viscosities which make them ideal candidates for tuning the viscosity of organic mixtures. Dow Corning 200 silicone (polydimethylsiloxane) oils, which are the most common silicon oil family, cover kinematic viscosities in the range 6.5×10^{-7}–1 m^2/s, but have associated RIs in the relatively narrow range 1.375–1.404, as shown in Fig. 13. Viscosity and RI tuning can then be achieved through mixing with a range of available miscible higher RI silicone oils like Dow Corning 550 (RI = 1.490–1.500, viscosity 1.0×10^{-4}–1.50×10^{-4} m^2/s), Dow Corning 556 (RI = 1.46, viscosity 2.25×10^{-5} m^2/s), or Dow Corning 710 (RI = 1.533, viscosity 5×10^{-3} m^2/s).

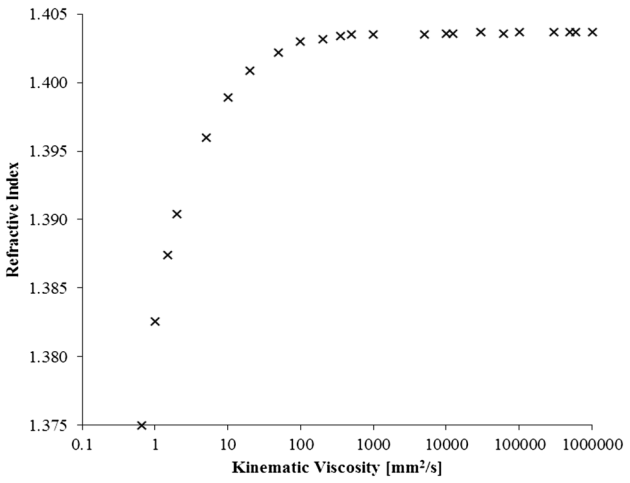

Fig. 13 Variation of RI with viscosity for Dow Corning 200 (polydimethylsiloxane) silicone oils (Dow Corning datasheets)

Finally, solubility in water (indicated in Table 7) and in other organic solvents should be checked when considering a liquid–liquid RIM system. Hassan and Dominguez-Ontiveros (2008) matched the RI of soda-lime glass to two different organic systems: (i) diethylphthalate; and (ii) a mixture of isopropanol and methylnaphthalene. Isopropanol, however, is fully soluble in water and, therefore, organic mixtures that include isopropanol cannot be used when water is the aqueous phase in a liquid–liquid system. UCON polyalkylene glycol based oils are also widely found in RIM-based experimental literature, but are again miscible with water.

4.2 Aqueous and hydrophilic liquids

Aqueous systems are comprised of water, which has a relatively low RI (of 1.333). This means that RI matching to the majority of available and commonly used solids and organic liquids, which have considerably higher RIs (hydrogels, FEP and fluorocarbons being exceptions), is a challenge and requires significant amounts of tuning with mixing or additives. An increase in the RI of an aqueous phase is often achieved through the addition of glycerol (Bailey and Yoda 2003; Takamura et al. 2012). Glycerol has a relatively high RI (of 1.473), thereby allowing a range of RI values to be spanned based on the water–glycerol ratio. At the same time, the dynamic viscosity of pure glycerol is 1.412 Pa s, so the addition of glycerol to water (0.89 mPa s) is also accompanied by a significant increase in viscosity. This increase in viscosity can be undesirable when studying liquid–liquid flows that mimic real flow systems, as the water-to-oil viscosity ratios can be significantly altered (Morgan et al. 2013, 2016). In such cases, glycerol solutions can be further combined with alcohols in ternary systems (Moreira et al. 2009) or salts, so that density, viscosity, or surface tension can be independently controlled. Baldwin et al. (1989) created a mixture of 79 vol% saturated NaI solution, 20 vol% glycerol, and 1 vol% water which matched the RI of PMMA, while also having approximately the same viscosity of blood.

The density and surface tension of glycerol solutions can also be modified via the addition of certain alcohols, e.g., ethanol, which has a significantly lower surface tension and density ($\sigma = 23.4 \times 10^{-3}$ N/m; $\rho = 789$ kg/m^3), but similar viscosity and RI ($\mu = 1.2 \times 10^{-3}$ Pa s; $n = 1.361$) compared to water (Vazquez et al. 1995; Khattab et al. 2012; Mathie et al. 2013; Markides et al. 2016). Nevertheless, ethanol is known to attack some plastics (e.g., PMMA), so chemical compatibly should be checked at the experiment design stage. Table 8 lists common liquids suitable for the RI tuning of aqueous solutions, where we have again included PMMA compatibility data that have been collated from supplier datasheets.

Table 8 Hydrophilic liquids previously used in RIM experiments, with their RI, surface tension, dynamic viscosity, and density

Liquid	n_L	Density (kg/m^3)	Dynamic viscosity* (mPa s)	Surface tension (mN/m)	PMMA compatibility	References
Water	1.333	998	1.04 at 20 °C	72.5	Good	Takamura et al. (2012)
Methanol	1.327	789	0.544 at 25 °C	22.07	Poor	Hayes (2015) Albuquerque et al. (1996)
Ethanol	1.360	785	1.082 at 25 °C	27.1	Poor	Gómez et al. (2006) Hayes (2015)
1,2 Propanedoil	1.432	1036	56.0 at 20 °C		Good	Smedley and Coles (1990)
Ethylene glycol	1.432	1109	19.9 at 20 °C		Good	Smedley and Coles (1990)
Dipropylene glycol	1.440	1021	76.2 at 20 °C		Good	Smedley and Coles (1990)
1,3 Propanedoil	1.440	1060	46.6 at 20 °C		Good	Smedley and Coles (1990)
Diethylene glycol	1.447	1116	35.7 at 20 °C		Good	Smedley and Coles (1990)
Formamide	1.447	1133	3.85 at 20 °C		Good	Smedley and Coles (1990)
1,5 Pentanediol	1.449	992	128.1 at 20 °C		Good	Smedley and Coles (1990)
Triethylene glycol	1.453	1124	49.0 at 20 °C		Good	Smedley and Coles (1990)
Tetraethylene glycol	1.459	1125	47.4			Stephenson and Stewart (1986)
Glycerol	1.474	1231	1500 at 20 °C	63.5	Good	Takamura et al. (2012)
Dimethylsulfoxide (DMSO)	1.477	1095	1.984 at 25 °C	42.92 at 25 °C	Poor	Baragi et al. (2005) Hayes (2015)

* Temperature for viscosity is provided when stated; otherwise, it is assumed that this is at ambient laboratory conditions between 20 and 25 °C

Salts are commonly added to increase the RI of aqueous RIM systems (see Table 9). The ability of salts to increase RI is usually limited by their solubility in the solvent, so the RI of a given solution can be modified from that of the pure liquid (e.g., water with RI of 1.333) up to that achieved by the saturated salt solution. Nevertheless, this solubility can be altered by further additives, such as crown ethers (Lopez-Gejo et al. 2007). On the other hand, the introduction of salts also leads to an increase in the density and viscosity of the resulting aqueous solution, as well as an increase in the risk of corrosion (e.g., electrochemical oxidation of metals), and therefore, care must be taken when selecting the materials to be used in any experimental campaign (e.g., plastics and, in particular, metals). The typical criteria for the selection of a given salt additive are: (i) increase in the RI with concentration; (ii) salt solubility; (iii) increase in the viscosity with concentration; (iv) increase in the density with concentration; (v) compatibility and corrosion potential; and (vi) stability of a given salt solution.

Table 9 List of solids used for RI tuning of aqueous solutions

Liquid	Solubility (g/100 g at 20 °C)	n_L	PMMA compatibility	References
Potassium dihydrogen phosphate (KH_2PO_4)	>10	1.330–1.345		Alahyari and Longmire (1994)
Sodium chloride (NaCl)	35.9	1.330–1.380	Good	Hayes (2015)
Caesium bromide (CsBr)	123 (at 25 °C)	1.330–1.405		Li et al. (2013)
Calcium chloride ($CaCl_2$)	74.5	1.330–1.442	Good	Hayes (2015)
Zinc chloride ($ZnCl_2$)	395	1.330–1.470	Good	Stöhr et al. (2003)
Sodium thiocyanate (NaSCN)	139	1.330–1.480		Budwig (1994)
Potassium thiocyanate (KSCN)	224	1.330–1.490		Jan et al. (1989)
Sodium salicylate ($C_7H_5NaO_3$)	125	1.330–1.490	Good	Prasad et al. (1991)
Sucrose ($C_{12}H_{22}O_{11}$)	~2000	1.330–1.490	Good	Dijksman et al. (2012)
Sodium iodide (NaI)	178	1.330–1.499	Good	Bai and Katz (2014)
Ammonium thiocyanate (NH_4SCN)	170	1.330–1.503	Good	Borrero-Echeverry and Morrison (2016)
Sodium polytungstate ($Na_6[H_2W_{12}O_{40}]$)	>1000	1.330–1.550	Good	Dijksman et al. (2012)
Zinc iodide (ZnI_2)	432	1.330–1.620	Good	Hendriks and Aviram (1982)

All these criteria are temperature sensitive making temperature control important especially in saturated systems where drops in temperature can lead to salts leaving the solution.

Referring to Table 9, the present review of the literature has revealed that NaI is the most widely employed salt in RIM experiments. Typical NaI solutions matching the RI of PMMA have concentrations in the range of 60.0–64.8 wt%, yielding a RI in the range 1.485–1.491 (Imao et al. 1996; Parker and Merati 1996; Uzol et al. 2002; Mehta et al. 2007; Uzol et al. 2007; Soranna et al. 2008; Yuki et al. 2008; Wu et al. 2009; Amatya and Longmire 2010; Wu et al. 2011, 2012; Yuki et al. 2011; Yuan et al. 2012; Tomac and Gregory 2014). A detailed study of the use of NaI for RI matching (aimed at PIV measurements) over an even wider RI range (1.330–1.510) was performed by Bai and Katz (2014), who also matched NaI solutions to three optical solids formed from resins with RIs in the range 1.495–1.508. NaI solutions with RIs >1.499 could only be reached at temperatures >23 °C. Of interest in the context of RI matching is a useful study by Narrow et al. (2000), who developed a model for predicting the RI of NaI solutions for a known temperature and concentration. At the same time, the addition of NaI to water does not significantly affect the liquid solution's viscosity. NaI solutions have kinematic viscosities of ~1.1×10^{-6} m^2/s, which is only slightly higher than that of water that has a viscosity of 1.0×10^{-6} m^2/s at 20 °C (Uzol et al. (2002, 2007). NaI like many iodides undergoes photodissociation, oxidizing in the presence of light (Chen and Fan 1992). This can, however, be counteracted through the addition of 0.1 g of sodium thiosulfate ($Na_2S_2O_3$) per L (Ghatage et al. 2014; Narrow et al. 2000; Parker and Merati 1996). The precipitation of iodide can also be reduced by the addition of 20 mg of ascorbic acid per cm^3 of salt solution (Jacobs et al. 1988).

NH_4SCN is the second most common salt reported in RIM systems and was examined in detail in the context of RIM experiments by Borrero-Echeverry and Morrison (2016). This study reported an RI value of 1.503 for a 62.6 wt% aqueous-NH_4SCN solution, also with a relatively low kinematic viscosity of 1.7 mm^2 s and a density of 1140 kg m^{-3}. NH_4SCN is, like other thiocyanates, toxic if inhaled or ingested and it is important that it is handled with care and suitable protective clothing.

Hendriks and Aviram (1982) investigated the use of ZnI_2 in RIM systems. It was shown that ZnI_2 can form aqueous solutions with a high RI (1.620) at 81 wt%, with a kinematic viscosity just over 5×10^{-6} m^2/s at 21 °C, and that for a less concentrated 60 wt% solution, the viscosity falls to 2×10^{-6} m^2/s whilst matching the RI of PMMA at 1.490. Hence, ZnI_2 solutions have the potential to be utilized as aqueous RIM systems matching all solids from FEP to PS in RI. Nevertheless, ZnI_2 like many salts is hydroscopic and the accurate measurement of the weight of a given salt requires the salt to be dried first (Hendriks and Aviram 1982).

The material compatibility and corrosion issues associated with the use of salts have been addressed by a number of investigators. Cenedese and Viotti (1996) noted that $ZnCl_2$ corrodes aluminium and so opted instead to use glycerol in their RIM experiments. Similarly, Reddy et al. (2013) considered a 55 wt% NaI solution too corrosive, while a solution of 42 wt% KSCN and a solution of 45% NH_4SCN were both considered too corrosive and too toxic. Borrero-Echeverry and Morrison (2016) found that NH_4SCN solutions were compatible with 6061 aluminium alloy, anodized aluminium, 316 stainless steel, common plastics, and glass but corroded plain steel and 304 stainless steel. Furthermore, Stöhr et al. (2003) showed that a 58 wt% concentration of $ZnCl_2$ has a pH of about 2 and is, therefore, incompatible with PMMA and many fluorescent dyes. Bailey and Yoda (2003) were successful in creating a ternary mixture of NH_4SCN, water, and glycerol that was compatible with plastics including PMMA, PC, and PVC. However, it corroded many metals, with the exception of 304 stainless steel and some aluminium alloys. In a couple of other approaches of interest; Dijksman et al. (2012) noted that sodium polytungstate is a relatively non-toxic salt, forming solutions with RIs up to 1.550 which are compatible with most plastics and metals, with the exception of aluminium, while Prasad et al. (1991) matched sodium salicylate solution to PMMA in static conditions. Sodium salicylate, however, was not deemed suitable for flow experiments, as it required high concentrations, was expensive and changed colour over time.

5 Conclusions

This review paper presented a number of previously employed refractive-index-matched experimental systems (solid and liquid combinations) reported in the literature, covering more than 280 references. Although the primary focus is on optical properties, information is included on broader experimental design aspects, including safety, toxicity, material compatibility, the role of temperature, wavelength, solubility/miscibility, as well as the use of liquid mixtures and/or additives (e.g., salts) for the tuning/adjustment of properties such as density, viscosity, and surface/interfacial tension. The practice of refractive-index matching forms an important component of the accurate and reliable application of optical experimental methods such as direct photography, laser-induced fluorescence, laser Doppler velocimetry or phase Doppler anemometry, particle image or tracking velocimetry (and variants thereof), and others, to a variety of multiphase flows that include

solid–liquid, liquid–liquid, and solid–liquid–liquid systems, with similar issues applying to internal or external single-phase (liquid) flows in confined solid spaces or over solid obstacles. This overview has shown that aqueous and organic phases can, in principle, be matched over a wide range of refractive indices (1.330–1.620), as well as varying viscosities, densities, and even surface and interfacial tensions. Further refractive-index tuning, through mixing of liquids or the addition of salts into solutions, can also be used for optical matching with improved accuracy, and can also allow the simultaneous tuning of other desirable properties, such as viscosity and density, for the purpose of attaining flow similarity. In the context of employing optical measurement methods, including advanced optical-based flow diagnostic techniques, the use of these refractive-index matching techniques is important in minimizing distortions in either illumination and/or detection caused by refractive-index differences between individual phases, increasing the overall accuracy of the measurements, as well as allowing for measurements in more complex (e.g., dispersed liquid–liquid) interfacial flows.

The liquid–liquid system matches reported in the literature were found to be concentrated near a refractive index of ~ 1.40, predominantly using silicone oils as the organic phase and glycerol–water solutions as the aqueous phase. With regard to solid materials, borosilicate glass and PMMA were found to be the most commonly employed solids in refractive-index-matched experiments, but these have high refractive indices (1.474 and 1.490, respectively) compared to water (1.333). Lower refractive-index-materials have been employed, such as FEP (1.338) and silicone rubbers (1.410–1.440), but these are less common. In particular, FEP and hydrogels are close matches for pure water, while silicone rubbers are a good option when creating flexible (compliant) models of biological or other structures. The use of solids with refractive indices between 1.333 and 1.410 is rare, but desirable, as this does not necessitate the use of additives to the aqueous phase for refractive-index tuning and matching. Suitable solids that can optically match the aforementioned liquid–liquid systems do exist, including for example fluoropolymers such as ETFE (1.403); however, we have not identified instances of the use of such plastics being reported within the literature. Therefore, an especially promising, compatible, non-hazardous, and readily available solid–liquid–liquid RIM system matched at ~1.40 uses ETFE, a silicone oil, and a ~50 wt% glycerol solution. Importantly, this system allows tuning of the liquid viscosity ratios due to the wide range of viscosities of silicone oils at RIs of ~1.40, and the ability to vary the glycerol–water mixing ratio. A second solid–liquid–liquid combination is that of FEP, water, and perfluoroperhydrophenanthrene, which is based on pure substances rather than mixtures. This relatively unusual combination is of particular interest, since the RIs of its three phases are all at or close to that of water (1.33–1.34), that in fact it includes. Depending on the accuracy required, this combination may not require any further tuning (mixing, additives) or adjustment (e.g., by temperature or otherwise). To the best of the authors' knowledge, neither of these two solid/liquid combinations have been previously reported in experimental multiphase flow investigations.

Acknowledgements This work has been undertaken within the Consortium on Transient and Complex Multiphase Flows and Flow Assurance (TMF). The authors gratefully acknowledge the contributions made to this project by the UK Engineering and Physical Sciences Research Council (EPSRC) through a Programme Grant (MEMPHIS, EP/K003976/1) and the following: ASCOMP; BP Exploration; Cameron Technology and Development; CD adapco; Chevron; KBC (FEESA); FMC Technologies; INTECSEA; Granherne; Institutt for Energiteknikk (IFE); Kongsberg Oil and Gas Technologies; MSi Kenny; Petrobras; Schlumberger Information Solutions; Shell; SINTEF; Statoil; and TOTAL.

Compliance with ethical standards

Conflict of interest SFW is an employee of Cameron, a Schlumberger company. IZ is an employee of Dantec Dynamics.

References

Abbas MA, Crowe CT (1987) Experimental study of the flow properties of a homogenous slurry near transitional Reynolds numbers. Int J Multiph Flow 13:357–364

Abbott JR (1991) Experimental observations of particle migration in concentrated suspensions: couette flow. J Rheol 35:773–795

Ackerson BJ, Pusey PN (1988) Shear-induced order in suspensions of hard spheres. Phys Rev Lett 61:1033–1036

Adrian RJ (1986) Multi-point optical measurements of simultaneous vectors in unsteady flow—a review. Int J Heat Fluid Flow 7:127–145

Adrian RJ (1991) Particle-imaging techniques for experimental fluid mechanics. Annu Rev Fluid Mech 23:261–304

Agrawal Y, Talbot L, Gong K (1978) Laser anemometer study of flow development in curved circular pipes. J Fluid Mech 85:497–518

Akinci A, Cobanoglu E (2009) Coating of Al mould surfaces with polytetrafluoroethylene (PTFE), fluorinated ethylene propylene (FEP), perfluoro-alkoxy (PFA) and ethylene-tetrafluoroethylene (ETFE). E Polym 33:1–7

Alahyari A, Longmire EK (1994) Particle image velocimetry in a variable density flow: application to a dynamically evolving microburst. Exp Fluids 17:434–440

Alahyari AA, Longmire EK (1997) Concentration measurements in experimental microbursts. AIAA J 35:569–571

Albrecht HE, Damaschke N, Borys M, Tropea C (2003) Laser Doppler and phase Doppler measurement techniques. Springer, Berlin

Albuquerque L, Ventura C, Gonçalves R (1996) Refractive indices, densities, and excess properties for binary mixtures containing methanol, ethanol, 1,2-ethanediol, and 2-methoxyethanol. J Chem Eng Data 41:685–688

Amatya DM, Longmire EK (2010) Simultaneous measurements of velocity and deformation in flows through compliant diaphragms. J Fluids Struct 26:218–235

Amini N, Hassan YA (2009) Measurements of jet flows impinging into a channel containing a rod bundle using dynamic PIV. Int J Heat Mass Transf 52:5479–5495

Amini N, Hassan YA (2012) An investigation of matched index of refraction technique and its application in optical measurements of fluid flow. Exp Fluids 53:2011–2020

Amundsen L (2011). An experimental study of oil-water flow in horizontal and inclined pipes. PhD thesis, Norwegian Univeristy of Science and Technology, Trondheim

Arago D, Biot J (1806) Mémoire sur les affinités des corps pour la lumière, et particulièrement sur les forces réfringentes des différens gaz. Académie des Sciences, Paris

Arroyo MP, Greated CA (1991) Stereoscopic particle image velocimetry. Meas Sci Technol 2:1181–1186

Augier F, Morchain J, Guiraud P, Masbernat O (2003) Volume fraction gradient-induced flow patterns in a two-liquid phase mixing layer. Chem Eng Sci 58:3985–3993

Augier FDR, Guiraud P, Masbernat O (2007) Fluctuating motion in a homogeneous liquid–liquid dispersed flow at high phase fraction. Phys Fluids 19:057105

Averbakh A, Shauly A, Nir A, Semiat R (1997) Slow viscous flows of highly concentrated suspensions—Part I: laser-Doppler velocimetry in rectangular ducts. Int J Multiph Flow 23:409–424

Aziza ARA, Wong KFV (2003) Velocity measurements across fluid-porous medium interface using particle image velocimetry. Int J Model Simul 23:179–186

Bai K, Katz J (2014) On the refractive index of sodium iodide solutions for index matching in PIV. Exp Fluids 55:1704

Bailey BC, Yoda M (2003) An aqueous low-viscosity density- and refractive index-matched suspension system. Exp Fluids 35:1–3

Baldwin JT, Tarbell JM, Deutsch S, Geselowitz DB (1989) Mean flow velocity patterns within a ventricular assist device. ASAIO J 35:429–432

Baldwin JT, Deutsch S, Geselowitz DB, Tarbell JM (1994) LDA measurements of mean velocity and Reynolds stress fields within an artificial heart ventricle. J Biomech Eng 116:190–200

Bale-Glickman J, Selby K, Saloner D, Savas O (2003) Experimental flow studies in exact-replica phantoms of atherosclerotic carotid bifurcations under steady input conditions. J Biomech Eng 125:38–48

Baragi JG, Aralaguppi MI, Aminabhavi TM, Kariduraganavar MY, Kittur AS (2005) Density, viscosity, refractive index, and speed of sound for binary mixtures of anisole with 2-chloroethanol, 1,4-dioxane, tetrachloroethylene, tetrachloroethane, DMF, DMSO, and diethyl oxalate at (298.15, 303.15, and 308.15) K. J Chem Eng Data 50:910–916

Begolo S, Colas G, Viovy JL, Malaquin L (2011) New family of fluorinated polymer chips for droplet and organic solvent microfluidics. Lab Chip 11:508–512

Berard LR, Raessi M, Bauer MT, Friedman PD, Codyer SR (2013) An investigation on the breakup of underwater buoyant oil jets: computational simulations and experiments. At Sprays 23:981–1000

Bhatia SC, Bhatia R, Dubey GP (2009) Refractive properties and internal pressures of binary mixtures of octan-1-ol with chloroform, 1,2-dichloroethane and 1,1,2,2-tetrachloroethane at 298.15 and 308.15 K. J Mol Liq 145:88–102

Blanchette F, Bigioni TP (2009) Dynamics of drop coalescence at fluid interfaces. J Fluid Mech 620:333–352

Bordoloi AD, Longmire EK (2012) Effect of neighboring perturbations on drop coalescence at an interface. Phys Fluids 24:062106

Borrero-Echeverry D, Morrison BCA (2016) Aqueous ammonium thiocyanate solutions as refractive index-matching fluids with low density and viscosity. Exp Fluids 57:123

Bovendeerd PHM, Steenhoven AAV, Vosse FNVD, Vossers G (1987) Steady entry flow in a curved pipe. J Fluid Mech 177:233–246

Bowman CL (1998) Quantifying the cleanliness of glass capillaries. Cell Biochem Biophys 29:203–223

Braun MJ, Canacci VA, Hendricks RC (1991) Flow visualization and quantitative velocity and pressure measurements in simulated single and double brush seals. Tribol Trans 34:70–80

Breedveld LVA (2000) Shear-induced self-diffusion in concentrated suspensions. PhD thesis, Universiteit Twente, Enschede

Breedveld V, Van Den Ende D, Tripathi A, Acrivos A (1998) The measurement of the shear-induced particle and fluid tracer diffusivities in concentrated suspensions by a novel method. J Fluid Mech 375:297–318

Breedveld V, Van Den Ende D, Bosscher M, Jongschaap RJJ, Mellema J (2001) Measuring shear-induced self-diffusion in a counterrotating geometry. Phys Rev E 63:021403

Breedveld V, Van Den Ende D, Bosscher M, Jongschaap RJJ, Mellema J (2002) Measurement of the full shear-induced self-diffusion tensor of noncolloidal suspensions. J Chem Phys 116:10529

Buchhave P, George WK, Lumley JL (1979) The measurement of turbulence with the laser-Doppler anemometer. Annu Rev Fluid Mech 11:443–503

Buchmann NA, Yamamoto M, Jermy M, David T (2010) Particle image velocimetry (PIV) and computational fluid dynamics (CFD) modelling of carotid artery haemodynamics under steady flow: a validation study. J Biomech Sci Eng 5:421–436

Buchmann NA, Atkinson C, Jeremy MC, Soria J (2011) Tomographic particle image velocimetry investigation of the flow in a modeled human carotid artery bifurcation. Exp Fluids 50:1131–1151

Budwig R (1994) Refractive index matching methods for liquid flow investigations. Exp Fluids 17:350–355

Budwig R, Elger D, Hooper H, Slippy J (1993) Steady flow in abdominal aortic aneurysm models. J Biomech Eng 115:418–423

Burdett ID, Webb DR, Davies GA (1981) A new technique for studying dispersion flow, holdup and axial mixing in packed extraction columns. Chem Eng Sci 36:1915–1919

Burgmann S, Grosse S, Schröder W, Roggenkamp J, Jansen S, Gräf F, Büsen M (2009) A refractive index-matched facility for fluid–structure interaction studies of pulsatile and oscillating flow in elastic vessels of adjustable compliance. Exp Fluids 47:865–881

Butscher D, Hutter C, Kuhn S, Rudolf Von Rohr P (2012) Particle image velocimetry in a foam-like porous structure using refractive index matching: a method to characterize the hydrodynamic performance of porous structures. Exp Fluids 53:1123–1132

Byron ML, Variano EA (2013) Refractive-index-matched hydrogel materials for measuring flow-structure interactions. Exp Fluids 54:1456

Cadillon J, Saksena R, Pearlstein AJ (2016) Transparent, immiscible, surrogate liquids with matchable refractive indexes: increased range of density and viscosity ratios. Phys Fluids 28:127102

Carpenter CP, Kinkead ER, Geary DL, Sullivan LJ, King JM (1975) Petroleum hydrocarbon toxicity studies. Toxicol Appl Pharm 32:282–297

Cenedese A, Viotti P (1996) Lagrangian analysis of nonreactive pollutant dispersion in porous media by means of the particle image velocimetry technique. Water Resour Res 32:2329–2343

Chaudhuri P, Gao Y, Berthier L, Kilfoil M, Kob W (2008) A random walk description of the heterogeneous glassy dynamics of attracting colloids. J Phys Condens Mater 20:244126

Chen RC, Fan LS (1992) Particle image velocimetry for characterizing the flow structure in three-dimensional gas–liquid–solid fluidized beds. Chem Eng Sci 47:3615–3622

Chen RC, Kadambi JR (1990) LDV measurements of solid–liquid slurry flow using refractive index matching technique. Part Sci Technol 8:97–109

Chen RC, Kadambi JR (1995) Discrimination between solid and liquid velocities in slurry flow using laser Doppler velocimeter. Powder Technol 85:127–134

Chen RC, Reese J, Fan LS (1994) Flow structure in a three-dimensional bubble column and three-phase fluidized bed. AIChE J 40:1093–1104

Chen B, Mikami F, Nishikawa N (2005) Experimental studies on transient features of natural convection in particles suspensions. Int J Heat Mass Transf 48:2933–2942

Cho JS, Han S, Kim KH, Beag YW, Koh SK (2003) Surface modification of polymers by ion-assisted reaction. Thin Solid Films 445:332–341

Conan C, Masbernat O, Décarre S, Liné A (2007) Local hydrodynamics in a dispersed-stratified liquid–liquid pipe flow. AIChE J 53:2754–2768

Corino ER, Brodkey RS (1969) A visual investigation of the wall region in turbulent flow. J Fluid Mech 37:1–30

Crimaldi JP (2008) Planar laser induced fluorescence in aqueous flows. Exp Fluids 44:851–863

Cui MM, Adrian RJ (1997) Refractive index matching and marking methods for highly concentrated solid–liquid flows. Exp Fluids 22:261–264

Curran SJ, Black RA (2004) Quantitative experimental study of shear stresses and mixing in progressive flow regimes within annular-flow bioreactors. Chem Eng Sci 59:5859–5868

Czarske JW (2006) Laser Doppler velocimetry using powerful solid-state light sources. Meas Sci Technol 17:R71–R91

Daviero GJ, Roberts PJW, Maile K (2001) Refractive index matching in large-scale stratified experiments. Exp Fluids 31:119–126

De Silva IPD, Fernando HJS (1998) Experiments on collapsing turbulent regions in stratified fluids. J Fluid Mech 358:29–60

Dibble CJ, Kogan M, Solomon MJ (2006) Structure and dynamics of colloidal depletion gels: coincidence of transitions and heterogeneity. Phys Rev E 74:041403

Dietze GF, Al-Sibai F, Kneer R (2009) Experimental study of flow separation in laminar falling liquid films. J Fluid Mech 637:73–104

Diez FJ, Bernal LP, Faeth GM (2005) PLIF and PIV measurements of the self-preserving structure of steady round buoyant turbulent plumes in crossflow. Int J Heat Fluid Flow 26:873–882

Dijksman JA, Rietz F, Lorincz KA, Van Hecke M, Losert W (2012) Invited article: refractive index matched scanning of dense granular materials. Rev Sci Instrum 83:011301

Downie H, Holden N, Otten W, Spiers AJ, Valentine TA, Dupuy LX (2012) Transparent soil for imaging the rhizosphere. PLoS One 7:e44276

Dreisbach RR (1948) Applicability of the Eykman equation. Ind Eng Chem 40:2269–2271

Drobny JG (2006) Rapra review report 184: fluoroplastics. Rapra Technology Ltd, Shrewsbury

Duffy DC, McDonald JC, Schueller OJ, Whitesides GM (1998) Rapid prototyping of microfluidic systems in poly(dimethylsiloxane). Anal Chem 70:4974–4984

Duncan DD, Bargeron CB, Borchardt SE, Deters OJ, Gearhart SA, Mark FF, Friedman MH (1990) The effect of compliance on wall shear in casts of a human aortic bifurcation. J Biomech Eng 112:183–188

Durst F, Loy T (1985) Investigations of laminar flow in a pipe with sudden contraction of cross sectional area. Comput Fluids 13:15–36

Durst F, Melling A, Whitelaw JH (1976) Principles and practice of laser-Doppler anemometry. Academic Press, London

Durst F, Müller R, Jovanovic J (1988) Determination of the measuring position in laser-Doppler anemometry. Exp Fluids 6:105–110

Durst F, Jovanovic J, Sender J (1995) LDA measurements in the near-wall region of a turbulent pipe flow. J Fluid Mech 295:305–335

Durst F, Brenn G, Xu TH (1997) A review of the development and characteristics of planar phase-Doppler anemometry. Meas Sci Technol 8:1203–1221

Ebnesajjad S, Khaladkar PR (2005) Fluoropolymers applications in chemical processing industries—the definitive user's guide and databook. William Andrew Inc, New York

Egelhoff CJ, Budwig RS, Elger DF, Khraishi TA, Johansen KH (1999) Model studies of the flow in abdominal aortic aneurysms during resting and exercise conditions. J Biomech 32:1319–1329

Eykman JF (1895) Recherches réfractométriques (suite). Rec Trav Chim 14:185–202

Eyring H, Jhon MS (1969) Significant liquid structures. Wiley, New York

Fort T (1964) The wettability of a homologous series of nylon polymers. Adv Chem 43:302–309

Fort C, Fu CD, Weichselbaum NA, Bardet PM (2015) Refractive index and solubility control of para-cymene solutions for index-matched fluid–structure interaction studies. Exp Fluids 56:210

Forziati AF (1950) Refractive index as a function of wavelength for sixty API-NBS hydrocarbons. J Res Natl Bur Stand 44:RP2085

Frish MB, Webb WW (1981) Direct measurement of vorticity by optical probe. J Fluid Mech 107:173–200

Fu S, Biwole PH, Mathis C (2015) Particle tracking velocimetry for indoor airflow field: a review. Build Environ 87:34–44

Gao Y, Kilfoil ML (2007) Direct imaging of dynamical heterogeneities near the colloid-gel transition. Phys Rev Lett 99:078301

Geoghegan PH, Buchmann NA, Spence CJT, Moore S, Jermy M (2012) Fabrication of rigid and flexible refractive-index-matched flow phantoms for flow visualization and optical flow measurements. Exp Fluids 52:1331–1347

Georgalas I, Ladas I, Tservakis I, Taliantzis S, Gotzaridis E, Papaconstantinou D, Koutsandrea C (2011) Perfluorocarbon liquids in vitreoretinal surgery: a review of applications and toxicity. Cutan Ocul Toxicol 30:251–262

Ghatage SV, Peng Z, Sathe MJ, Doroodchi E, Padhiyar N, Moghtaderi B, Joshi JB, Evans GM (2014) Stability analysis in solid–liquid fluidized beds: experimental and computational. Chem Eng J 256:169–186

Gijsen FJH, Palmen DEM, Van Der Beek MHE, Van De Vosse FN, Van Dongen MEH, Janssen JD (1996) Analysis of the axial flow field in stenosed carotid artery bifurcation models—LDA experiments. J Biomech 29:1483–1489

Gladstone JH, Dale TP (1863) XIV Researches on the refraction, dispersion and sensitiveness of liquids. Philos Trans R Soc Lond 153:317–343

Goharzadeh A, Khalili A, Jørgensen BB (2005) Transition layer thickness at a fluid-porous interface. Phys Fluids 17:057102

Gómez E, González B, Calvar N, Tojo E, Domínguez Á (2006) Physical properties of pure 1-ethyl-3-methylimidazolium ethylsulfate and its binary mixtures with ethanol and water at several temperatures. J Chem Eng Data 51:2096–2102

Graham AL (1991) NMR imaging of shear-induced diffusion and structure in concentrated suspensions undergoing Couette flow. J Rheol 35:191–201

Graham AL, Bird RB (1984) Particle clusters in concentrated suspensions. 1. Experimental observations of particle clusters. Ind Eng Chem Fundam 23:406–410

Grant I (1997) Particle image velocimetry: a review. Proc Inst Mech Eng Part C J Mech Eng Sci 211:55–76

Gülan U, Lüthi B, Holzner M, Liberzon A, Tsinober A, Kinzelbac W (2012) Experimental study of aortic flow in the ascending aorta via particle tracking velocimetry. Exp Fluids 53:1469–1485

Haam SJ, Brodkey RS (2000) Motions of dispersed beads obtained by particle tracking velocimetry measurements. Int J Multiph Flow 26:1419–1438

Haam SJ, Brodkey RS, Fort I, Klaboch L, Placnik M, Vanecek V (2000) Laser Doppler anemometry measurements in an index of refraction matched column in the presence of dispersed beads. Int J Multiph Flow 26:1401–1418

Ham JM, Homsy GM (1988) Hindered settling and hydrodynamic dispersion in quiescent sedimenting suspensions. Int J Multiph Flow 14:533–546

Han H, Zhu Z, Gabriel K (2006) A study on the effect of gas flow rate on the wave characteristics in two-phase gas–liquid annular flow. Nucl Eng Des 236:2580–2588

Hannoun I (1985) Matching the refractive index in density stratified flows. California Institute of Technology, California

Hannoun IA, Fernando HJS, List EJ (1988) Turbulence structure near a sharp density interface. J Fluid Mech 189:189–209

Harrington M, Lin M, Nordstrom KN, Losert W (2014) Experimental measurements of orientation and rotation of dense 3D packings of spheres. Granul Matter 16:185–191

Hassan YA, Dominguez-Ontiveros EE (2008) Flow visualization in a pebble bed reactor experiment using PIV and refractive index matching techniques. Nucl Eng Des 238:3080–3085

Hayes WM (ed) (2015) CRC handbook of chemistry and physics, 96th edn. CRC Press, Boca Raton

Heller W (1945) The determination of refractive indices of colloidal particles by means of a new mixture rule or from measurements of light scattering. Phys Rev 68:5–10

Hendriks F, Aviram A (1982) Use of zinc iodide solutions in flow research. Rev Sci Instrum 53:75–78

Hewitt GF, Jayanti S, Hope CB (1990) Structure of thin liquid films in gas–liquid horizontal flow. Int J Multiph Flow 16:951–957

Hibberd DJ, Mackie AR, Moates GK, Penfold R, Watson AD, Barker GC (2007) Preparation and characterisation of a novel buoyancy and refractive index matched oil-in-water emulsion. Colloid Surf A 301:453–461

Hirsch D, Graff EC, Pereira F, Gharib M (2015) Influence of common transparent materials on the accuracy of image-based velocimetry. Meas Sci Technol 26:087002

Hopkins LM, Kelly JT, Wexler AS, Prasad AK (2000) Particle image velocimetry measurements in complex geometries. Exp Fluids 29:91–95

Huang AYL, Huang MYF, Capart H, Chen RH (2008) Optical measurements of pore geometry and fluid velocity in a bed of irregularly packed spheres. Exp Fluids 45:309–321

Huang AYL, Huang MYF, Chen RH, Capart H (2009a) Influence of aspect ratio on the distribution of porosity and velocity in columns of spheres. J Chin Inst Eng 32:421–426

Huang MYF, Huang AYL, Chen RH, Capart H (2009b) Automated tracking of liquid velocities in a refractive index matched porous medium. J Chin Inst Eng 32:877–882

Hydraulic-Institute (1979) Hydraulic institute engineering data book. Cleveland, OH

Im S, Heo GE, Jeon YJ, Sung HJ, Kim SK (2013) Tomographic PIV measurements of flow patterns in a nasal cavity with geometry acquisition. Exp Fluids 55:1644

Imao S, Itoh M, Harada T (1996) Turbulent characteristics of the flow in an axially rotating pipe. Int J Heat Fluid F 17:444–451

Isehunwa SO, Olanisebe EB, Ajiboye OO, Akintola SA (2015) Estimation of the refractive indices of some binary mixtures. Afr J Pure Appl Chem 10:58–64

Jacobs DA, Jacobs CW, Andereck CD (1988) Biological scattering particles for laser Doppler velocimetry. Phys Fluids 31:3457–3461

Jan DL, Shapiro AH, Kamm RD (1989) Some features of oscillatory flow in a model bifurcation. J Appl Physiol 67:147–159

Jana SC (1995) Apparent wall slip velocity coefficients in concentrated suspensions of noncolloidal particles. J Rheol 39:1123–1132

Johnston W, Dybbs A, Edwards R (1975) Measurement of fluid velocity inside porous media with a laser anemometer. Phys Fluids 18:913–914

Kang JH, Lee KJ, Nam JH, Kim CJ, Park HS, Lee S, Kwang I (2010) Visualization of invasion-percolation drainage process in porous media using density-matched immiscible fluids and refractive-index-matched solid structures. J Power Sources 195:2608–2612

Kapoor B, Acrivos A (2006) Sedimentation and sediment flow in settling tanks with inclined walls. J Fluid Mech 290:39–66

Karnis A, Goldsmith HL, Mason SG (1966) The kinetics of flowing dispersions I: concentrated suspensions of rigid particles. J Colloid Interf Sci 22:531–553

Kaufman LJ, Weitz DA (2006) Direct imaging of repulsive and attractive colloidal glasses. J Chem Phys 125:074716

Kaur S, Leal LG (2010) Drop deformation and break-up in concentrated suspensions. J Rheol 54:981–1008

Kefayati S, Poepping TL (2013) Transitional flow analysis in the carotid artery bifurcation by proper orthogonal decomposition and particle image velocimetry. Med Eng Phys 35:898–909

Kegel WK, Van Blaaderen A (2000) Direct observation of dynamical heterogeneities in colloidal hard-sphere suspensions. Science 287:290–293

Khattab IS, Bandarkar F, Fakhree MAA, Jouyban A (2012) Density, viscosity, and surface tension of water + ethanol mixtures from 293 to 323K. Korean J Chem Eng 29:812–881

Kim J, Longmire EK (2009) Investigation of binary drop rebound and coalescence in liquids using dual-field PIV technique. Exp Fluids 47:263–278

Kinsey JL (1977) Laser-induced fluorescence. Annu Rev Phys Chem 28:349–372

Koh CJ, Hookham P, Leal LG (1994) An experimental investigation of concentrated suspension flows in a rectangular channel. J Fluid Mech 266:1–32

Kohnen C, Bohnet M (2001) Measurement and simulation of fluid flow in agitated solid/liquid suspensions. Chem Eng Technol 24:639–643

Kollhoff RT, Kelemen K, Schuchmann HP (2015) Local multiphase flow characterization with micro particle image velocimetry using refractive index matching. Chem Eng Technol 38:1774–1782

Kondyurin A, Gan BK, Bilek MMM, Mizuno K, McKenzie DR (2006) Etching and structural changes of polystyrene films during plasma immersion ion implantation from argon plasma. Nucl Instrum Methods Phys Res Sect B Beam Interact Mater Atoms 251:413–418

Krishnan GP, Beimfohr S, Leighton DT (1996) Shear-induced radial segregation in bidisperse suspensions. J Fluid Mech 321:371–393

Krug D, Holzner M, Lüthi B, Wolf M, Tsinober A, Kinzelbach W (2014) A combined scanning PTV/LIF technique to simultaneously measure the full velocity gradient tensor and the 3D density field. Meas Sci Technol 25:065301

Kumar S, Kusakabe K, Fan LS (1993) Heat transfer in three-phase fluidized beds containing low-density particles. Chem Eng Sci 48:2407–2418

Kurtz SS, Ward AL (1936) The refractivity intercept and the specific refraction equation of Newton. I. Development of the refractivity intercept and comparison with specific refraction equations. J Frankl Inst 222:527–646

Le TB, Troolin DR, Amatya D, Longmire EK, Sotiropoulos F (2013) Vortex phenomena in sidewall aneurysm hemodynamics: experiment and numerical simulation. Ann Biomed Eng 41:2157–2170

Leighton D, Acrivos A (1987) Measurement of shear-induced self-diffusion in concentrated suspensions of spheres. J Fluid Mech 177:109–131

Leis AP, Schlicher S, Franke H, Strathmann M (2005) Optically transparent porous medium for nondestructive studies of microbial biofilm architecture and transport dynamics. Appl Environ Microbiol 71:4801–4808

Lenoble M, Snabre P, Pouligny B (2005) The flow of a very concentrated slurry in a parallel-plate device: influence of gravity. Phys Fluids 17:073303

Leron RB, Soriano AN, Li MH (2012) Densities and refractive indices of the deep eutectic solvents (choline chloride + ethylene glycol or glycerol) and their aqueous mixtures at the temperature ranging from 298.15 to 333.15 K. J Taiwan Inst Chem Eng 43:551–557

Li Y, Li SN, Zhai Q, Marcilla A, Jiang Y, Hu M (2013) Solubility, density, refractive index, and viscosity for the polyhydric alcohol + CsBr + H_2O ternary systems at different temperatures. J Chem Eng Data 58:1577–1588

Lichtenecker K (1926) Die dielektrizitätskonstante natürlicher und künstlicher mischkörper. Phys Z 27:115–158

Lichtenecker K, Rother K (1931) Die Herleitung des logarithmischen mischungsgesetzes aus allgemeinen prinzipien der stationären strömung. Phys Z 32:255–260

Liu L (2005) Optical and computational studies of liquid–liquid flows. PhD thesis, Imperial College London, London

Liu HT, Lin JT, Delisi DP, Robben FA (1977).Application of fluorescence technique to dye-concentration measurements in a turbulent jet. In: Proceedings of the symposium on flow measurement in open channels and closed conduits, Gaithersburg

Liu CH, Nouri JM, Whitelaw JH, Tse DGN (1989) Particle velocities in a swirling, confined flow. Combust Sci Technol 68:131–145

Liu CH, Vafidis C, Whitelaw JH, Margary R (1990) Flow in the coolant passages of an internal combustion engine cylinder head. Exp Fluids 10:50–54

Liu L, Matar OK, Hewitt GF (2006a) Laser-induced fluorescence (LIF) studies of liquid–liquid flows. Part II: flow pattern transitions at low liquid velocities in downwards flow. Chem Eng Sci 61:4022–4026

Liu L, Matar OK, Lawrence CJ, Hewitt GF (2006b) Laser-induced fluorescence (LIF) studies of liquid–liquid flows. Part I: flow structures and phase inversion. Chem Eng Sci 61:4007–4021

Longmire EK, Bordoloi AD (2015) Drop penetration through a constriction: effect of surrounding fluid. Proc IUTAM 15:194–200

Longmire EK, Norman TL, Gefroh DL (2001) Dynamics of pinch-off in liquid/liquid jets with surface tension. Int J Multiph Flow 27:1735–1752

Lopez-Gejo JL, Kunjappu J, Turro NJ, Conley WE (2007) Amplification of the index of refraction of aqueous immersion fluids with crown ethers. J Micro Nanolithogr MEMS MOEMS 6:013002

Lorentz HA (1906) Theory of electrons and its applications to the phenomena of light and radiant heat. GE Stechert & Co, New York

Lovick J, Angeli P (2004) Experimental studies on the dual continuous flow pattern in oil–water flows. Int J Multiph Flow 30:139–157

Lowe ML, Kutt PH (1992) Refraction through cylindrical tubes. Exp Fluids 13:315–320

Lyon MK, Leal LG (1998a) An experimental study of the motion of concentrated suspensions in two-dimensional channel flow. Part 1. Monodisperse systems. J Fluid Mech 363:25–56

Lyon MK, Leal LG (1998b) An experimental study of the motion of concentrated suspensions in two-dimensional channel flow. Part 2. Bidisperse systems. J Fluid Mech 363:57–77

Maas HG, Gruen A, Papantoniou D (1993) Particle tracking velocimetry in three-dimensional flows. Exp Fluids 15:133–146

Majithia AK, Hall S, Harper L, Bowen PJ (2008) Droplet breakup quantification and processes in constant and pulsed air flows. In: Proceedings of ILASS conference, Lake Como

Majumdar A, Graham AL, Roco MC, Stroeve P (1987) Experimental study on solid particle dynamics in shear flow. Powder Technol 49:217–226

Malitson IH (1963) A redetermination of some optical properties of calcium fluoride. Appl Opt 2:1103

Mandava S, Kolla N, Chagarlamudi K, Anne SB, Abbineni R (2015) Refractive properties for binary mixtures containing DEC + o-xylene or m-xylene or p-xylene. Int J Innov Res Sci Eng Technol 4:12598–12612

Markides CN, Mathie R, Charogiannis A (2016) An experimental study of spatiotemporally resolved heat transfer in thin liquid-film flows falling over and inclined heated foil. Int J Heat Mass Transf 93:872–888

Mathie R, Nakamura H, Markides CN (2013) Heat transfer augmentation in unsteady conjugate thermal systems—Part II: applications. Int J Heat Mass Transf 56:819–833

McCafferty E, Wightman JP (1999) Determination of the acid-base properties of metal oxide films and of polymers by contact angle measurements. J Adhes Sci Technol 13:1415–1436

McDougall TJ (1979) On the elimination of refractive-index variations in turbulent density-stratified liquid flows. J Fluid Mech 93:83–96

Mcilroy HM, Mceligot DM, Pink RJ (2010) Measurement of turbulent flow phenomena for the lower plenum of a prismatic gas-cooled reactor. Nucl Eng Des 240:416–428

Mehra R (2003) Application of refractive index mixing rules in binary systems of hexadecane and heptadecane with n-alkanols at different temperatures. J Chem Sci 115:147–154

Mehta M, Kadambi JR, Sastry S, Sankovic JM, Wernet MP, Addie G, Visintainer R (2007) Particle velocities in the rotating impeller of a slurry pump. In: 5th Joint ASME/JSME fluids engineering conference, San Diego

Merrington AC, Richardson EG (1947) The break-up of liquid jets. Proc Phys Soc 59:1–13

Mikami F, Chen B, Nishikawa N (2001) Visualization and PTV study of natural convection in particle suspensions. Simultaneous measurements of velocity, temperature and interface between particle-free fluid and suspension. JSME Int J Ser B 44:30–37

Miller P, Danielson K, Moody G, Slifka A, Drexler E, Hertzberg J (2006) Matching index of refraction using a diethyl phthalate/ethanol solution for in vitro cardiovascular models. Exp Fluids 41:375–381

Mohamed-Kassim Z, Longmire EK (2003) Drop impact on a liquid–liquid interface. Phys Fluids 15:3263–3273

Mohamed-Kassim Z, Longmire EK (2004) Drop coalescence through a liquid/liquid interface. Phys Fluids 16:2170–2181

Mondy LA, Graham AL, Majumdar A, Bryant LE (1986) Techniques of measuring particle motions in concentrated suspensions. Int J Multiph Flow 12:497–502

Moreira R, Chenlo F, Legall D (2009) Kinematic viscosity and refractive index of aqueous solutions of ethanol and glycerol. Ind Eng Chem Res 48:2157–2161

Morgan RG, Markides CN, Hale CP, Hewitt GF (2012) Horizontal liquid–liquid flow characteristics at low superficial velocities using laser-induced fluorescence. Int J Multiph Flow 43:101–117

Morgan RG, Markides CN, Zadrazil I, Hewitt GF (2013) Characteristics of horizontal liquid–liquid flows in a circular pipe using simultaneous high-speed laser-induced fluorescence and particle velocimetry. Int J Multiph Flow 49:99–118

Morgan RG, Ibarra R, Zadrazil I, Matar OK, Hewitt GF, Markides CN (2016) On the role of buoyancy-driven instabilities in horizontal liquid–liquid flow. Int J Multiph Flow 89:123–135

Moroni M, Cushman JH (2001) Three-dimensional particle tracking velocimetry studies of the transition from pore dispersion to Fickian dispersion for homogeneous porous media. Water Resour Res 37:873–884

Najjari MR, Hinke JA, Bulusu KV, Plesniak MW (2016) On the rheology of refractive-index-matched, non-Newtonian blood-analog fluids for PIV experiments. Exp Fluids 57:96

Narrow TL, Yoda M, Abdel-Khalik SI (2000) A simple model for the refractive index of sodium iodide aqueous solutions. Exp Fluids 28:282–283

Newton I (1704) Opticks: or, a treatise of the reflexions, refractions, inflexions and colours of light. Willliam Innys, London

Ng KM, Davis HT, Scriven LE (1978) Visualization of blob mechanics in flow through porous media. Chem Eng Sci 33:1009–1017

Nguyen TT, Biadillah DY, Mongrain R, Brunette J, Tardif JC, Bertrand OF (2004) A method for matching the refractive index and kinematic viscosity of a blood analog for flow visualization in hydraulic cardiovascular models. J Biomech Eng 126:529–535

Ni WJ, Capart H (2015) Cross-sectional imaging of refractive-index-matched liquid-granular flows. Exp Fluids 56:163

Nicolai HLN, Guazzelli E (1995) Effect of the vessel size on the hydrodynamic diffusion of sedimenting spheres. Phys Fluids 7:3–5

Nicolai H, Herzhaft B, Hinch EJ, Oger L, Guazzelli E (1995) Particle velocity fluctuations and hydrodynamic self-diffusion of sedimenting non-Brownian spheres. Phys Fluids 7:12–23

Nicolai HLN, Peysson Y, Guazzelli EL (1996) Velocity fluctuations of a heavy sphere falling through a sedimenting suspension. Phys Fluids 8:855–862

Ninomiya N, Yasuda K (2006) Visualization and PIV measurement of the flow around and inside of a falling droplet. J Vis 9:257–264

Northrup MA, Kulp TJ, Angel SM (1991) Fluorescent particle image velocimetry: application to flow measurement in refractive index-matched porous media. Appl Opt 30:3034–3040

Nouri JM, Whitelaw JH, Yianneskis M (1987) Particle motion and turbulence in dense two-phase flows. Int J Multiph Flow 13:729–739

Ortiz-Dueñas C, Kim J, Longmire EK (2010) Investigation of liquid–liquid drop coalescence using tomographic PIV. Exp Fluids 49:111–129

Oster G (1948) The scattering of light and its applications to chemistry. Chem Rev 43:319–365

Ottewill RH, Williams NSJ (1987) Study of particle motion in concentrated dispersions by tracer diffusion. Nature 325:232–234

Ovdat H, Berkowitz B (2006) Pore-scale study of drainage displacement under combined capillary and gravity effects in index-matched porous media. Water Resour Res 42:W06411

Pacák P, Kodejš Z (1988) Molar volumes and refractivities of highly concentrated solutions of ammonium and potassium thiocyanates in water and dimethylsulfoxide. Can J Chem 66:2244–2249

Park JT, Mannheimer RJ, Grimley TA, Morrow TB (1989) Pipe flow measurements of a transparent non-Newtonian slurry. J Fluids Eng 111:331–336

Parker J, Merati P (1996) An investigation of turbulent Taylor–Couette flow using laser Doppler velocimetry in a refractive index matched facility. J Fluids Eng 118:810–818

Pashtrapanska M, Jovanović J, Lienhart H, Durst F (2006) Turbulence measurements in a swirling pipe flow. Exp Fluids 41:813–827

Patil VA, Liburdy JA (2010) Refractive index matching with distortion measurements in a bed of irregularly packed spheres. In: Proceedings of ASME 3rd joint US-European fluids engineering summer meeting and 8th international conference on nanochannels, microchannels, and minichannels, Montreal

Patil VA, Liburdy JA (2012) Optical measurement uncertainties due to refractive index mismatch for flow in porous media. Exp Fluids 53:1453–1468

Patil VA, Liburdy JA (2013) Turbulent flow characteristics in a randomly packed porous bed based on particle image velocimetry measurements. Phys Fluids 25:043304

Perktold K, Hofer M, Rappitsch G, Loew M, Kuban BD, Friedman MH (1997) Validated computation of physiologic flow in a realistic coronary artery branch. J Biomech 31:217–228

Peterson DA, Tankin R, Bankoff SG (1987) Bubble behavior in a three-phase fluidized bed. Int J Multiph Flow 13:477–491

Peurrung LM, Rashidi M, Kulp TJ (1995) Measurement of porous medium velocity fields and their volumetric averaging characteristics using particle tracking velocimetry. Chem Eng Sci 50:2243–2253

Pielhop K, Klaas M, Schröder W (2012) Analysis of the unsteady flow in an elastic stenotic vessel. Eur J Mech B Fluids 35:102–110

Polling BE, Prausnitz JM, O'Connell JP (2001) The properties of gases and liquids. McGraw-Hill Inc, New York

Pouplin A, Masbernat O, Décarre S, Liné A (2011) Wall friction and effective viscosity of a homogeneous dispersed liquid–liquid flow in a horizontal pipe. AIChE J 57:1119–1131

Prasad V, Brown K, Tian Q (1991) Flow visualization and heat transfer experiments in fluid-superposed packed beds heated from below. Exp Therm Fluid Sci 4:12–24

Rashidi M, Peurrung L, Tompson AFB, Kulp TJ (1996) Experimental analysis of pore-scale flow and transport in porous media. Adv Water Resour 19:163–180

Ravelet F, Delfos R, Westerweel J (2007) Experimental studies of liquid–liquid dispersion in a turbulent shear flow. In: 11th EUROMECH European turbulence conference, Porto

Reddy RK, Sathe MJ, Joshi JB, Nandakumar K, Evans GM (2013) Recent developments in experimental (PIV) and numerical (DNS) investigation of solid–liquid fluidized beds. Chem Eng Sci 92:1–12

Reis JC, Lampreia IM, Santos AF, Moita ML, Douheret G (2010) Refractive index of liquid mixtures: theory and experiment. ChemPhysChem 11:3722–3733

Rheims J, Köser J, Wriedt T, (1997) Refractive-index measurements in the near-IR using an Abbe refractometer. Meas Sci Technol 8:601–605

Richards JR, Scheele GF (1985) Measurement of laminar jet velocity distributions in liquid–liquid systems using flash photolysis. Chem Eng Commun 36:73–92

Saarinen V, Karesoja M, Kallio T, Paronen M, Kontturi K (2006) Characterization of the novel ETFE-based membrane. J Membr Sci 280:20–28

Saksena R, Christensen KT, Pearlstein AJ (2015) Surrogate immiscible liquid pairs with refractive indexes matchable over a wide range of density and viscosity ratios. Phys Fluids 27:087103

Saleh S, Thovert JF, Adler PM (1992) Measurement of two-dimensional velocity fields in porous media by particle image displacement velocimetry. Exp Fluids 12:210–212

Satake SI, Aoyagi Y, Unno N, Yuki K, Seki Y, Enoeda M (2015) Three-dimensional flow measurement of a water flow in a sphere-packed pipe by digital holographic PTV. Fusion Eng Des 98–99:1864–1867

Schäfer M, Höfken M, Durst F (1997) Detailed LDV measurements for visualization of the flow field within a stirred-tank reactor equipped with a rushton turbine. Chem Eng Res Des 75:729–736

Schmidt FW, Kulakowski B, Wang DF (1984) Evaluation of the effect of variable refraction index on the path of a laser beam. Exp Fluids 2:153–158

Scholz P, Reuter I, Heitmann D (2012) PIV measurements of the flow through an intake port using refractive index matching. In: 16th International symposium on applications of laser techniques to fluid mechanics, Lisbon

Sharma S, Patel PB, Patel RS, Vora JJ (2007) Density and comparative refractive index study on mixing properties of binary liquid mixtures of eucalyptol with hydrocarbons at 303.15, 308.15 and 313.15 K. Eur J Chem 4:343–349

Shauly A, Averbakh A, Nir A, Semiat R (1997) Slow viscous flows of highly concentrated suspensions—Part II: particle migration, velocity and concentration profiles in rectangular ducts. Int J Multiph Flow 23:613–629

Shuib AS, Hoskins PR, Easson WJ (2010) Flow regime characterization in a diseased artery model. World Acad Sci Eng Technol 4:87–91

Simpkin R (2010) Derivation of Lichtenecker's logarithmic mixture formula from Maxwell's equations. IEEE Trans Microw Theory Tech 58:545–550

Smedley G, Coles D (1990) Some transparent immiscible liquid pairs. J Colloid Interface Sci 138:42–60

Soranna F, Chow YC, Uzol O, Katz J (2008) Turbulence within a turbomachine rotor wake subject to nonuniform contraction. AIAA J 46:2687–2702

Stephenson JL, Stewart WE (1986) Optical measurements of porosity and fluid motion in packed beds. Chem Eng Sci 41:2161–2170

Stöhr M, Roth K, Jähne B (2003) Measurement of 3D pore-scale flow in index-matched porous media. Exp Fluids 35:159–166

Stoots C, Becker S, Condie K, Durst F, Mceligot D (2001) A large-scale matched index of refraction flow facility for LDA studies around complex geometries. Exp Fluids 30:391–398

Svensson FJE, Rasmuson A (2004) LDA-measurements in a stirred tank with a liquid–liquid system at high volume percentage dispersed phase. Chem Eng Technol 27:335–339

Svensson FJE, Rasmuson A (2006) PIV measurements in a liquid–liquid system at volume percentages up to 10% dispersed phase. Exp Fluids 41:917–931

Takamura K, Fischer H, Morrow NR (2012) Physical properties of aqueous glycerol solutions. J Petrol Sci Eng 98–99:50–60

Tasić AZ, Djordjevic BD, Grozdanic DK, Radojkovic N (1992) Use of mixing rules in predicting refractive indexes and specific refractivities for some binary liquid mixtures. J Chem Eng Data 37:310–313

Thormahlen I, Straub J, Grigull U (1985) Refractive index of water and its dependence on wavelength, temperature and density. J Phys Chem Ref Data 14:933–945

Tidhar M, Merchuk JC, Sembira AN, Wolf D (1986) Characteristics of a motionless mixer for dispersion of immiscible fluids—II. Phase inversion of liquid–liquid systems. Chem Eng Sci 41:457–462

Timberlake BD, Morris JF (2002) Concentration band dynamics in free-surface Couette flow of a suspension. Phys Fluids 14:1580–1589

Tindal MJ, Cheung RS, Yianneskis M (1988) Velocity characteristics of steady flows through engine inlet ports and cylinders. SAE Technol Pap Ser 880383:1–19

Tomac MN, Gregory JW (2014) Internal jet interactions in a fluidic oscillator at low flow rate. Exp Fluids 55:1730

Tropea C (1995) Laser Doppler anemometry: recent developments and future challenges. Meas Sci Technol 6:605–619

Ueda T, Tanaka H (1975) Measurements of velocity, temperature and velocity fluctuation distributions in falling liquid films. Int J Multiph Flow 2:261–272

Unno N, Nakata S, Satake S-I, Taniguchi J (2016) Three-dimensional particle tracking around microstructures in water via total internal reflection fluorescence microscopy and refractive-index-matching method. Exp Fluids 57:120

Uzol O, Chow YC, Katz J, Meneveau C (2002) Unobstructed particle image velocimetry measurements within an axial turbo-pump using liquid and blades with matched refractive indices. Exp Fluids 33:909–919

Uzol O, Brzozowski D, Chow YC, Katz J, Meneveau C (2007) A database of PIV measurements within a turbomachinery stage and sample comparisons with unsteady RANS. J Turbul 8:N10

Varty RL (1984) A new system for index-matched laser-anemometer measurements. J Phys E Sci Instrum 17:1124–1126

Vazquez G, Alvarez E, Navaza JM (1995) Surface tension of alcohol water + water from 20 to 50 °C. J Chem Eng Data 40:611–614

Walker DA (1987) A fluorescence technique for measurement of concentration in mixing liquids. J Phys E Sci Instrum 20:217–224

Walker JD, Tiederman WG, Phillips WM (1989) Effect of tilting disk, heart valve orientation on flow through a curved aortic model. J Biomech Eng 111:228

Wang DC, Khalili A (2002) Flow visualization and quantitative measurements inside porous media by particle image velocimetry. In: Proceedings of SPIE optical technology and image processing for fluids and solids diagnostics, Beijing

Wang P, Song C, Briscoe C, Makse HA (2008) Particle dynamics and effective temperature of jammed granular matter in a slowly sheared three-dimensional Couette cell. Phys Rev E 77:061309

Weitzman JS, Samuel LC, Craig AE, Zeller RB, Monismith SG, Koseff JR (2014) On the use of refractive-index-matched hydrogel for fluid velocity measurement within and around geometrically complex solid obstructions. Exp Fluids 55:1862

Wiederseiner S, Andreini N, Epely-Chauvin G, Ancey C (2011) Refractive-index and density matching in concentrated particle suspensions: a review. Exp Fluids 50:1183–1206

Wiener O (1910) Zur theorie der refraktionskonstanten. Ber Verh Koniglich Saechs Ges Wiss Leipzig, Math-Phys Kl 62:256–277

Wildman DJ, Ekmann JM, Kadambi JR, Chen RC (1992) Study of the flow properties of slurries using the refractive index matching technique LDV. Powder Technol 73:211–218

Wu Y, Yuan H, Shao J, Liu S (2009) Experimental study on internal flow of a mini centrifugal pump by PIV measurement. Int J Fluid Mach Syst 2:121–126

Wu Y, Liu S, Yuan H, Shao J (2011) PIV measurement on internal instantaneous flows of a centrifugal pump. Sci Chin Technol Sci 54:270–276

Wu H, Miorini RL, Tan D, Katz J (2012) Turbulence within the tip-leakage vortex of an axial waterjet pump. AIAA J 50:2574–2587

Yagi T, Sato A, Shinke M, Takahashi S, Tobe Y, Takao H, Murayama Y, Umezu M (2013) Experimental insights into flow impingement in cerebral aneurysm by stereoscopic particle image velocimetry: transition from a laminar regime. J R Soc Interface 10:20121031

Yarlagadda AP, Yoganathan AP (1989) Experimental studies of model porous media fluid dynamics. Exp Fluids 8:59–71

Yousif MY, Holdsworth DW, Poepping TL (2010) A blood-mimicking fluid for particle image velocimetry with silicone vascular models. Exp Fluids 50:769–774

Yuan HJ, Shao J, Wu YL, Liu SH (2012) Experiment of a centrifugal pump during changing speed operation. IOP Conf Ser Earth Environ Sci 15:62–65

Yuki K, Okumura M, Hashizume H, Toda S, Morley NB, Sagara A (2008) Flow visualization and heat transfer characteristics for sphere-packed pipes. J Thermophys Heat Transf 22:632–648

Yuki K, Hasegawa S, Sato T, Hashizume H, Aizawa K, Yamano H (2011) Matched refractive-index PIV visualization of complex flow structure in a three-dimensionally connected dual elbow. Nucl Eng Des 241:4544–4550

Zachos A, Kaiser M, Merzkirch W (1996) PIV measurements in multiphase flow with nominally high concentration of the solid phase. Exp Fluids 20:229–231

Zadrazil I, Markides CN (2014) An experimental characterization of liquid films in downwards co-current gas–liquid annular flow by particle image and tracking velocimetry. Int J Multiph Flow 67:42–53

Zadrazil I, Bismarck A, Hewitt GF, Markides CN (2012) Shear layers in the turbulent pipe flow of drag reducing polymer solutions. Chem Eng Sci 72:142–154

Zadrazil I, Matar OK, Markides CN (2014) An experimental characterization of downwards gas–liquid annular flow by laser-induced fluorescence: flow regimes and film statistics. Int J Multiph Flow 60:87–102

Zerai B, Saylor BZ, Kadambi JR, Oliver MJ, Mazaheri AR, Ahmadi G, Bromhal GS, Smith DH (2005) Flow characterization through a network cell using particle image velocimetry. Transp Porous Medium 60:159–181

Zhang J, Li J, Han Y (2004) Superhydrophobic PTFE surfaces by extension. Macromol Rapid Commun 25:1105–1108

Zhao Y, Markides CN, Matar OK, Hewitt GF (2013) Disturbance wave development in two-phase gas–liquid upwards vertical annular flow. Int J Multiph Flow 55:111–129

Zhu W, Knapp Y, Deplano V (2016) Low hazard refractive index and density-matched fluid for quantitative imaging of concentrated suspensions of particles. Exp Fluids 57:68

Zisselmar R, Molerus O (1979) Investigation of solid–liquid pipe flow with regard to turbulence modification. Chem Eng J 18:233–239